DMAP and HMTA manganese(III) meso-tetraphenylporphyrin-based coordination complexes: Syntheses, physicochemical properties, structural and biological activities

H. Mkacher, F.B. Taheur, N. Amiri, A. Almahri, F. Loiseau, F. Molton, E.M. Vollbert, T. Roisnel, I. Turowska-Tyrk, H. Nasri

DMAP and HMTA Manganese(III) *meso*-Tetraphenylporphyrin-based coordination complexes: Syntheses, Physicochemical Properties, Structural and Biological activities

Hayfa Mkacher [a], Fadia Ben Taheur [b], Nesrine Amiri [a], Albandary Almahri [c], Frédérique Loiseau [d], Florian Molton [d] Emiliano Martinez Vollbert [d], Thierry Roisnel [e], Ilona Turowska-Tyrk [f] and Habib Nasri *[a]

[a]: University of Monastir, Laboratory of Physical chemistry of Materials, Faculty of Science of Monastir, Avenue of environment, 5019 Monastir, Tunisia.
[b]: Laboratory of Analysis, Treatment and Valorization of Environmental Pollutants and Products, Faculty of Pharmacy, Monastir University, Tunisia.
[c]: Department of Chemistry, College of Science and Humanities in Al-Kharj, Prince Sattam Bin Abdulaziz University, Al-Kharj 11942, Saudi Arabia.
[d]: Department of Molecular Chemistry, CNRS UMR 5250, Université Grenoble Alpes, F-38000 Grenoble, France.
[e]: Institute of Chemical Sciences of Rennes, UMR 6226, University of Rennes 1, Beaulieu Campus, 35042 Rennes, France.
[f]: Faculty of Chemistry, Wrocław University of Science and Technology, Wybrzeże Wyspiańskiego 27, 50-370 Wrocław, Poland.

Abstract

The reactions of the (triflato)(*meso*-tetra(*para*-methoxyphenyl)porphyrinato)manganese(III) ([Mn^{III}(TMPP)(SO_3CF_3)] complex with an excess of 4-dimethylaminopyridine (DMAP) and hexamethylenetetramine (HMTA) have been examined. These reactions yield crystalline [Mn^{III}(TMPP)$(DMAP)_2$](0.1Cl)(0.9SO_3CF_3)·2$CHCl_3$ (**I**) and [Mn^{III}(TMPP)$(HMTA)_2$](SO_3CF_3)·2CH_2Cl_2 (**II**) complexes, respectively. The hyper *d-type* electronic spectra of **I-II** are characteristic for high-spin (S = 2) Mn(III) metalloporphyrins with very redshifted Soret bands. A cyclic voltammetry investigation was carried out on these two Mn(III) coordination compounds. The crystal structures of the solid complexes **I-II** were determined by X-ray single-crystal diffraction and elucidated by Hirshfeld surface approach. Furthermore, bioactivity of the H_2TMPP free base, the [Mn^{III}(TMPP)(SO_3CF_3)] starting material and complexes **I-II**, was assessed by a set of *in vitro* tests checking for antioxidant, antibacterial and antifungal (against several strains) effects.

* Corresponding author:
Fax: +216 20 720 809.
E-mail address: hnasri1@gmail.com and habib.nasri@fsm.rnu.tn (Habib Nasri).

Keywords: Manganese(III) porphyrin complexes; X-ray molecular structure; UV/Vis spectroscopy; Cyclic voltammetry; Biological activities.

1-Introduction

For more than a century porphyrin and porphyrin metal complexes, known as metalloporphyrins, have attracted considerable interest after the pioneering works of Willstatter and Fischer [1,2]. These tetrapyrrolic aromatic compounds have been first used as models for hemoproteins and over the years, a great deal of concerted efforts has brought to light substantial understanding of the structure-function of synthetic porphyrins and metalloporphyrins. It is noteworthy that since the report of the synthetic methods of porphyrins by Adler-Longo in 1967 [3] and Lindsey in 1986 with yields ca. and above 20%, the number of published investigations of porphyrinic compounds kept growing exponentially. In addition, metal complex porphyrins and porphyrin-like species such as expanded porphyrins [4] have been used in the area of catalysis [5,6] nonlinear optics, solar energy conversion and in a number of medical applications such as in photodynamic therapy (PDT) of cancers [7,8]. On the other hand, manganese porphyrins have been of interest to many researchers after the pioneering work of Boucher [9–12]. In the early 1960s and the 1970s, the great interest in these metalloporphyrins stemmed from *(i)* the role of manganese in the release of oxygen from water in photocatalysis reactions [13] and *(ii)* the important catalytic properties of these compounds which can mimic those of P450 cytochromes [14] functionalization of both unsaturated and saturated hydrocarbons as well as more complex molecules. Thereby, Groves *et al* [15], reported that catalytic amounts of the manganese porphyrin [Mn^{III}(TPP)Cl], in the presence of iodosylbenzene mediated the efficient oxygenation of cyclohexane to afford cyclohexanol as the major product. In 2017, Groves *et al.,* reported an investigation concerning the selective C-H functionalization of aliphatic molecules [16]. More recently, in 2020, it has been reported by Mo *et al.*[17], the use of coordinated and grafted manganese porphyrin to mesoporous and macroporous chitosan as catalyst in the oxidation of ethylbenzene.

Notably, the center ion in manganese metalloporphyrins is present in the II, III, IV and V oxidation states and up to date, 43, 201, 5 and 3 Mn(II), Mn(III), Mn(IV) and Mn(V) porphyrin complex structures are respectively reported in the Cambridge Structural Database (CSD Version 5.42, last update April 2021) [18]. The large number of published manganese(III) porphyrin structures testifies to the high stability of these compounds under ambient laboratory conditions. It has been noticed that Mn(III) metalloporphyrins can be coordinated to one or two axial ligands and the majority of these $3d^4$ complexes are high-spin for which the ground state electronic configuration of the Mn(III) center metal is $[(d_{xy})^1(d_{xz})^1(d_{yz})^1(d_{z^2})^1]$. The majority of these Mn(III) high-spin metalloporphyrins are neutral pentacoordinate type [Mn^{III}(Porph)X] where X is an ionic monodentate ligand such as Cl^-, Br^-, NO_2^-, NO_3^-, OAc^- and TCA^- (trichloroacetate) [19–22]. Manganese(III) high-spin porphyrin complexes are also present as six-coordinated porphyrin cations type $[Mn^{III}(Porph)(L)_2]^+$, Y^- where Y^- is the counterion and L designates N-donor or O-donor neutral axial ligand such as: pyridine, imidazole piperidine and dimethylformamide

(DMF) [23]. Furthermore, several structures of hexacoordinated high-spin Mn(III) neutral porphyrin complexes type [Mn^{III}(Porph)X(L)] (X = ionic ligand and L = neutral monodentate ligand)] have been reported, e.g. [Mn^{III}(TPP)Cl(py)] and [Mn^{III}(TPP)Cl(DABCO)] [23].

On the other hand, in the last decade, several investigations on antibacterial antifungal activities of porphyrins and metalloporphyrins have been reported [24–27]. Nevertheless, no antibacterial or antifungal activities using manganese metalloporphyrins studies are so far reported in the literature.

In this work and in continuation on our studies on the synthesis and characterization of metalloporphyrins, we report herein our investigation concerning the reaction of 4-dimethylaminopyridine (DMAP) and hexamethylenetetramine (HMTA) axial ligands with the (triflato)(*meso*-tetra(*para*-methoxyphenyl)porphyrinto)manganese(III) ([Mn^{III}(TMPP)(SO_3CF_3)] leading to the bis(4-dimethylaminopyridine)[(*meso*-tetra(*para*-methoxyphenyl)porphyrinto)]manganese(III) (**I**) and the bis(hexamethylenetetramine)[(*meso*-tetra(*para*-methoxyphenyl)porphyrinto)]manganese(III) (**II**) ion complexes. The UV/Vis, IR, and cyclic voltammetry characterization of **I-II** as well as the X-ray molecular structure and the Hirshfeld surface analysis of these two high-spin (S =2) Mn(III) porphyrins are reported. Furthermore, the antibacterial, antifungal and antioxidant activities of **I-II**, the H_2TMPP free base porphyrin and the [Mn^{III}(TMPP)(SO_3CF_3)] starting material were also performed.

2. Experimental Section

2.1. Materials and methods

All reagents employed were commercially available and were used as received without further purification. All manipulations were carried out under aerobic conditions. The synthesis of the *meso*-tetra(*para*-methoxyphenyl)porphyrin (H_2TMPP) was performed according to the Adler – Longo method [3].

Spectroscopy UV/Vis and IR: The UV/Vis spectra were recorded with a WinASPECT PLUS (validation for SPECORD PLUS version 4.2) scanning spectrophotometer. Fourier-transformed IR spectra were recorded on a PerkinElmer Spectrum Two FT-IR spectrometer.

Electrochemistry: Cyclic voltammetry (CV) experiments were performed with a CH-660B potentiostat (CH Instruments). All analytical experiments were conducted at room temperature under an argon atmosphere (argon stream) in a standard one-compartment, three-electrode electrochemical cell. Tetra-n-butylammonium perchlorate (TBAP) was used as the supporting electrolyte (0.2 M) in dichloromethane previously distilled over calcium hydride under argon. An automatic Ohmic drop compensation procedure was systematically implemented before the CV data were recorded with electrolytic solutions containing the studied compounds at concentrations of ca. 10^{-3} M. CH Instruments vitreous carbon (ϕ = 3 mm) working

electrodes were polished with 1 µm diamond paste before each recording. The $Ag/AgNO_3$ 0.01 M (TBAP 0.2 in CH_2Cl_2) redox couple was used as the reference electrode. The potential of the ferrocene/ ferrocenium redox couple was used as an internal reference (86 mV vs. $Ag/AgNO_3$ under our experimental conditions). For comparison with previously published data, all potentials given in the text and in Table 5 have been converted to values relative to the Saturated Calomel Electrode (SCE) by using the following relationship: $E(SCE) = E(Ag/AgNO_3) + 298$ mV.

2.2. Synthesis

The *meso*-tetra(*para*-methoxyphenyl)porphyrin (H_2TMPP) was prepared by using the Alder and Longo method [3].

2.2.1 Synthesis of [Mn^{III}(TMPP)(OAc)]

In a 100 mL one-necked balloon, H_2TMPP (240 mg, 0.330 mmol) was dissolved in DMF (30 mL) with an excess of $Mn(OAc)_2.4H_2O$ (240 mg, 0.98 mmol). The reaction was refluxed under magnetic stirring for 4 hours at 150°C. The mixture was washed with water and after filtration the obtained precipitate was dried under vacuum. The solid was crystallized using chloroform / n-hexane to get dark green solid (232 mg, yield 83%). $C_{50}H_{39}MnN_4O_6$ (846.82) Calcd: C 70.92, H 4.64, N 6.62, found: C 71.57, H 4.81, N 6.86; UV/Vis (CH_2Cl_2): λ_{max} (logε) = 382(5.98), 407(5.96), 482(6.08), 586(5.42), 624(5.44). IR (solid, cm^{-1}): 2996-2853 [ν(CH) porphyrin], 1713 [ν(C=O, OAc)], 1244 [ν(C-O, OAc)], 998 [δ(CCH) porphyrin].

2.2.2. Synthesis of [Mn^{III}(TMPP)(SO_3CF_3)]

The synthesis of the [Mn^{III}(TMPP)(SO_3CF_3)] starting material was carried out under argon. In a Schlenk tube containing [Mn^{III}(TMPP)(OAc)] (232 mg, 0.274 mmol) and silver triflate (1.1 eq, 0.301 mmol, 49,46 mg) was added 80 mL of distilled THF. The reaction mixture was stirred at room temperature overnight. After filtration, the solvent was removed using rotavapor and dried under vacuum, then the crude product was crystallized from n-hexane to get a pure dark green solid (252 mg, yield 98%). $C_{49}H_{36}F_3MnN_4O_7S$ (936.83) Calcd: C 62.82, H 3.87, N 5.98, found: C 63.21, H 3.98, N 6.12; UV/Vis (CH_2Cl_2): λ_{max} (logε) = 394(6.09), 410(6.06), 481(6.08), 577(5.53), 614(5.56). IR (solid, cm^{-1}): 3417 [ν(OH) H_2O], 2960-2853 [ν(CH) porphyrin], 1290, 1024, 1246, 1174, 633-603, 514 [$\nu_{as}(SO_3)$, $\nu_s(SO_3)$, $\nu_s(CF_3)$, $\nu_{as}(CF_3)$, $\delta(CF_3)$, $\delta(SO_3)$], 998 [δ(CCH) porphyrin].

2.2.3. Synthesis of complexes I-II

[Mn^{III}(TMPP)(SO_3CF_3)] (20 mg, 0.024 mmol) was mixed with an excess of the N-donor ligands 4-dimethylaminopyridine (DMAP) and hexamethylenetetramine (HMTA) (13.4 equiv., 0.214 mmol) in 5 mL

of chloroform for **I** and dichloromethane for **II**, respectively. The reaction mixture was stirred at room temperature for 1 h. Crystals of the desired complex were obtained by slow diffusion of n-hexane into the chloroform or dichloromethane solution respectively (complex **I**: 28 mg, yield 85%, complex **II**: 31 mg, yield 92%)

Complex **I** ($C_{64.9}H_{58}N_8MnCl_{6.1}F_{2.7}O_{6.7}S_{0.9}$) (1408.58) Calcd: C 55.34, H 4.15, N 7.96, found: 54.42, H 4.29, N 8.11; UV/Vis (CH_2Cl_2): λ_{max} (logε) = 394(6.02), 410(5.99), 483(6.05), 579(5.40), 617(5.45). IR (solid, cm^{-1}): 3002 [ν(CH) DMAP], 2927-2834 [ν(CH) porphyrin], 1268, 1241-1227, 1175-1150, 1026, 564-558, 533-524 [$\nu_{as}(SO_3)$, $\nu_s(CF_3)$, $\nu_{as}(CF_3)$, $\nu_s(SO_3)$, $\delta(CF_3)$, $\delta(SO_3)$], 998 [δ(CCH) porphyrin].

Complex **II** ($C_{63}H_{64}F_3Cl_4MnN_{12}O_7S$) (1387.09) Calcd: C 54.55, H 4.65, N 12.12, found: 54.73, H 4.83, N 12.39; UV/Vis (CH_2Cl_2): λ_{max} (logε) = 396(6.08), 418(6.03), 488(6.05), 588(5.53), 626(5.62).
IR (solid, cm^{-1}): 2950-2844 [ν(CH) porphyrin, HMTA], 1489-1460 [$\nu(CH_2)$ HMTA], 1283, 1244, 1174, 1024, 557-514 [$\nu_{as}(SO_3)$, $\nu_s(CF_3)$, $\nu_{as}(CF_3)$, $\nu_s(SO_3)$, $\delta(CF_3)$, $\delta(SO_3)$], 998 [δ(CCH) porphyrin].

2.3. Biological Studies

2.3.1. Antibacterial screening

Pathogenic strains were cultivated on nutrient agar at 37 °C for 24 h, then, pure colonies were suspended in 10 mL of 0.9% sterile saline solution then mixed for 5 min. Suspensions were adjusted to 0.5 McFarland standard turbidity. 1 mL of bacterial suspension was spread over Mueller Hinton Agar medium plates and incubated for 30 min at 37°C. Then, 6 mm diameter wells were dug in agar medium using sterile glassy borer. The studied compounds were prepared in DMSO (1 mg/mL) leading to a final concentration of 10^{-5} M and were introduced into the respective wells. One of the wells was supplemented with DMSO as control). The plates were placed in a 37°C incubator for 24 h to allow bacterial growth. After 24 h, the diameters of the clear zone of inhibition surrounding the sample were measured in millimeters by digital caliper.

2.3.2. Antifungal activity

Yeasts Strains: three yeasts strains, Candida krusei ATCC6258, Candida albicans ATCC90028 and Cryptococcus neoformans ATCC14116 were cultured on Sabouraud agar at 37°C for 48 h. Then, pure colonies were suspended in 10 mL of 0,9% sterile saline solution, mixed well for 5 min and suspensions were adjusted to 0.5 McFarland standard turbidity. 1 mL of yeast suspension was spread over Sabouraud agar medium plates and incubated for 30 min at 37 °C. Then, 6 mm diameters wells were dug in agar medium using sterile glassy borer. The studied species were prepared in DMSO (1 mg/mL) and introduced

into the respective wells, one of the wells was supplemented with DMSO as control. The plates were placed in a 37 °C incubator for 48 h to allow yeast growth. After 48 h, the diameters of the clear zone of inhibition surrounding the sample were measured in millimeters by digital caliper.

Fungal Strains: three fungi strains, Aspergillus flavus 15UA005, Aspergillus niger 15UA006 and Aspergillus fumigatus ATCC204305 were cultured on inclined Sabouraud agar in Falcon tube 15 mL at 25 °C for 7 days. The spore of fungal strain was suspended in peptone water and counted to have 106 spores/mL. Then, 1 mL of fungal suspension was spread over Sabouraud agar medium plates and incubated for 30 min at 25 °C. Then, 6 mm diameter wells were dug in agar medium using sterile glassy borers. The studied compounds were prepared in DMSO (1 mg/mL) and introduced into the respective wells, one of the wells was supplemented with DMSO as control. The plates were placed in a 25 °C incubator for five days to allow fungal growth. The diameters of the clear zone of inhibition surrounding the sample were measured in millimeters by digital caliper.

2.3.3. Antioxidant activity

• **DPPH free radical scavenging assay:** The DPPH (2,2-diphenyl-1-picrylhydrazyl) and the ABTS (2,2'-azinobis-(3-ethylbenzothiazoline-6-sulfonic acid) were used to evaluate the antioxidant activity of the H_2TMPP free base porphyrin, the [Mn^{III}(TMPP)(SO_3CF_3)] starting material and complexes **I-II**.

For this investigation we used the 25 µg, 50 µg, 75 µg and 100 µg/ml concentrations of our four porphyrinic species. We mixed 2 mL of the porphyrinic sample with 2 mL of 0.1 M of a sodium acetate buffer solution (pH = 5.5) and 1 mL of a methanol DPPH solution (0.5 M) was added. This mixture was shaken and left in the dark for 30 min then, using a WinASPECT PLUS spectrophotometer, the absorbance was measured at 517 nm. Equation 1 (Eq. 1) were used to calculate the percentage of radical scavenging activity (RSA %):

$$RSA\ \% = [(AC - AS)/AC] \times 100 \qquad \text{(Eq. 1)}$$

where the AS is the absorbance, and the AC is the absorbance of control of the sample.

The IC50 (in µg/mL) which is the required concentration to scavenge 50% of free radicals was calculated for each sample for comparison using equation 2 (Eq. 2):

$$\%\ Inhibitor\ ABTS = \left(A_o - \frac{A_1}{A_o}\right) x100 \qquad \text{(Eq. 2)}$$

where: - A_1 = the absorption of the sample

- A_o = the absorption of reference (Vitamin C is used as standard)

• **ABTS free radical scavenging assay:**

The production of ABTS radical cations (ABTS+•) was made by reacting 0.17 mM of a $K_2S_2O_8$ (potassium persulfate) aqueous solution with a ABTS (2,2'-azinobis-(3-ethylbenzothiazoline-6-sulfonic acid) aqueous stock solution (2 mM) at room temperature in the dark for 16 hours.

The absorption was measured at 734 nm (using a blank at 734 nm) and before use, the solution containing the ABTS radical cations was diluted with ethanol to get an absorbance of 0.700 ± 0.020. For each porphyrinic sample, various DMSO concentrations (25 µg, 50 µg, 75 µg and 100 µg/ml) were added to the ABTS solution. The ABTS scavenging ability was given in term of IC50 (Eq. 2) value while the percentage of radical scavenging was calculated using Eq. 1.

2.4. X-ray structure determination

The X-ray intensity data for **I-II** were collected at 150 K with D8 VENTURE Bruker AXS and APEXII Bruker-AXS diffractometers, respectively. These two diffractometers are equipped with a CCD camera and a graphite-monochromator. The X-ray radiation used was the Mo-Kα radiation (λ = 0.71073 Å). The intensity data for **I-II** were collected by the narrow-frame method at low temperature. Both unit cell parameters for **I-II** were calculated and then refined from the full data collections. The reflections were scaled and corrected for absorption effects using the SADABS program version (Bruker APEX2 2014) [28]. For **II**, the counterion is made by one full triflate ion $(SO_3CF_3)^-$ but for **I**, the counterion is mostly made by $SO_3CF_3^-$ with an occupancy factor or 90% and a minor occupancy of 10% is made by a chloride ion. The hydrogen atoms were placed in calculated positions and treated as riding on their parent atoms. The crystallographic data, the structural refinement details, and selected bond lengths and angles for **I-II** are reported in Tables 1 and 2.

Table 1. Crystal data and structural refinements for **I-II**.

	I	**II**
Formula	$C_{64.9}H_{58}Cl_{6.1}F_{2.7}MnN_8O_{6.7}S_{0.9}$	$C_{63}H_{64}Cl_4F_3MnN_{12}O_7S$
Crystal System	monoclinic	triclinic
Crystal	$P2_1/c$	$P\text{-}1$
a (Å)	14.0868(16)	10.8335(6)
b (Å)	11.8283(13)	11.9920(6)
c (Å)	39.210(5)	14.0142(8)
α (°)	90.00	107.320(2)
β (°)	94.961(4)	96.831(2)
γ (°)	90.00	110.833(2)
V (Å^3)	6508.8(13)	1572.05(15)
Z	4	1
ρcalc./ g cm-3	1.437	1.465
X-ray radiation	Mo Kα	Mo Kα
μ/ mm^{-1}	0.549	0.486
F(000)	2898	718
Crystal size (mm^3)	0.38 x 0.06 x 0.06	0.40 x 0.30 x 0.17
Crystal Color	black	blue
Crystal Shape	stick	prism
T (K)	150(2)	150(2)
θ_{min} - θ_{max} (°)	2.085- 25.000	2.078 - 27.242
Limiting indices	-16 ≤ h ≤ 16, -13 ≤ k ≤ 14 -46 ≤ l ≤ 46	-13 ≤ h ≤ 14, -15 ≤ k ≤ 13 -15 ≤ l ≤ 18
R(int)	0.0361	0.0323

Reflections collected/unique	56701 / 11432	20995 / 7035
Observed data [$I_o > 2\sigma(F_o)$]	9615	5479
Parameters/Rest	825 / 0	412 / 0
S [all data]	1.025	1.027
R_1[a], wR_2[c] [$F_o > 4\sigma(F_o)$]	R_1 = 0.0593, wR_2 = 0.1395	R_1 = 0.0426, wR_2 = 0.0991
[all data]	R_1 = 0.0721, wR_2 = 0.1473	R_1 = 0.0626, wR_2 = 0.1111
Min./max. res. (eÅ^{-3})	1.277 / -1.067	0.819/-0.651
CCDC	2144173	2165563

[a]: $R_1 = \Sigma||F_o| - |F_c||/\Sigma|F_o|$, [b]: $wR_2 = \{\Sigma[w(|F_o|^2 - |F_c|^2)^2]/\Sigma[w(|F_o|^2)^2]\}^{1/2}$.

Table 2. Selected bond distances (Å) and angles (°) in the molecular structures of complexes **I-II**.

I

Manganese (III) coordination polyhedron of **I**

Mn-N1	2.016(2)	N1-Mn-N5	90.96(10)
Mn-N2	2.016(3)	N2-Mn-N5	90.75(10)
Mn-N3	2.021(3)	N3-Mn-N5	89.94(10
Mn-N4	2.024(3)	N4-Mn-N5	89.86(10
Mn-N5	2.308(3)	N1-Mn-N7	88.31(10)
Mn-N7	2.324(3)	N2-Mn-N7	92.06(10)
N1-Mn-N2	89.54(10	N3-Mn-N7	90.81(10)
N1-Mn-N3	178.99(11)	N4-Mn-N7	87.32(10)
N1-Mn-N4	90.51(10)	N5-Mn-N7	177.08(10)
N2-Mn-N3	90.00(10)	N3-Mn-N4	89.94(10)
N2-Mn-N4	179.38(11)		

DMAP axial ligands of **I**

N5-C53	1.342(4)	N7-C56	1.345(4)
C53-C52	1.377(5)	C56-C57	1.371(5)
C52-C51	1.411(5)	C57-C58	1.409(5)
C51-C50	1.411(5)	C58-C59	1.402(5)
C50-C49	1.375(5)	C59-C60	1.369(5)
C51-N6	1.354(5)	C58-N8	1.358(4)
N6-C54	1.450(5)	N8-C61	1.448(5)
N6-C55	1.460(5)	N8-C62	1.451(5)
C49-N5-C53	115.5(3)	C60-N7-C56	115.1(3)
C50-C51-C52	119.7(3)	C57-C58-C59	115.8(3)
N6-C51-C50	121.9(3)	C58-N8-C61	121.7(3)
C54-N6-C55	119.1(3)	C61-N8-C62	117.4(3)

II

Manganese (III) coordination polyhedron of **II**

Mn-N1	2.006(2)
Mn-N2	2.012(2)
Mn-N3	2.439(2)
N1-Mn-N2	90.12(7)
N1-Mn-N5	90.68(6)
N2-Mn-N5	89.47(6)

HMTA axial ligand coordination polyhedron of **II**

N3-C25	1.489(3)	C30-N3	1.488(3)
C25-N4	1.462(3)	C25-N3-Mn	111.15(12)
N4-C26	1.459(4)	C29-N3-Mn	113.37(12)
C26-N5	1.468(3)	C30-N3-Mn	110.98(12)
N5-C27	1.465(3)	C25-N3-C29	107.15(18)
C27-N6	1.465(3)	C25-N3-C30	107.40(19)
N6-C30	1.462(3)	C29-N3-C30	113.37(12)

2.5. Hirshfeld surface analysis

The Crystal Explorer17.5 program has been utilized to obtain the Hirshfeld surfaces and the 2D Fingerprint plots of our two manganese(III) porphyrin complexes **I-II** [20] based on the crystallographic CIF (Crystallographic Information File). Equation 3 was used to calculate the different normalized contact distances "d_{norm}" where "d_e" is the distance from the point to the nearest nucleus external to the surface, "d_i" is the distance to the nearest nucleus internal to the surface and "vdW" is the van der Waals radii of the atom [24].

$$d_{norm} = \frac{d_i - r_i^{vdW}}{r_i^{vdW}} + \frac{d_e - r_e^{vdW}}{r_e^{vdW}} \qquad \text{(Eq. 3)}$$

3. Results and Discussion

3-1. Synthesis of I-II

The triflate manganese(III) $[Mn^{III}(TMPP)(SO_3CF_3)]$ complex was used as starting material because the triflate is known to be easily substituted by other neutral or anionic ligands. The reaction of $[Mn^{III}(TMPP)(SO_3CF_3)]$ with an excess of 4-dimethylaminopyridine (DMAP) and hexamethylenetetramine (HMTA) in chloroform and dichloromethane, respectively leads to the hexacoordinated complexes **I-II** (Scheme 1). According to the X-ray diffraction study, the formula of **I** and **II** are: $[Mn^{III}(TMPP)(DMAP)_2](0.9SO_3CF_3)(0.1Cl)\cdot 2CHCl_3$ (**I**) and $[Mn^{III}(TMPP)(HMTA)_2](SO_3CF_3)\cdot 2CH_2Cl_2$ (**II**) respectively. The presence of the chloride ion (as 10% of the total counterion moiety) in the lattice of **I** could come from the chloroform used as solvent.

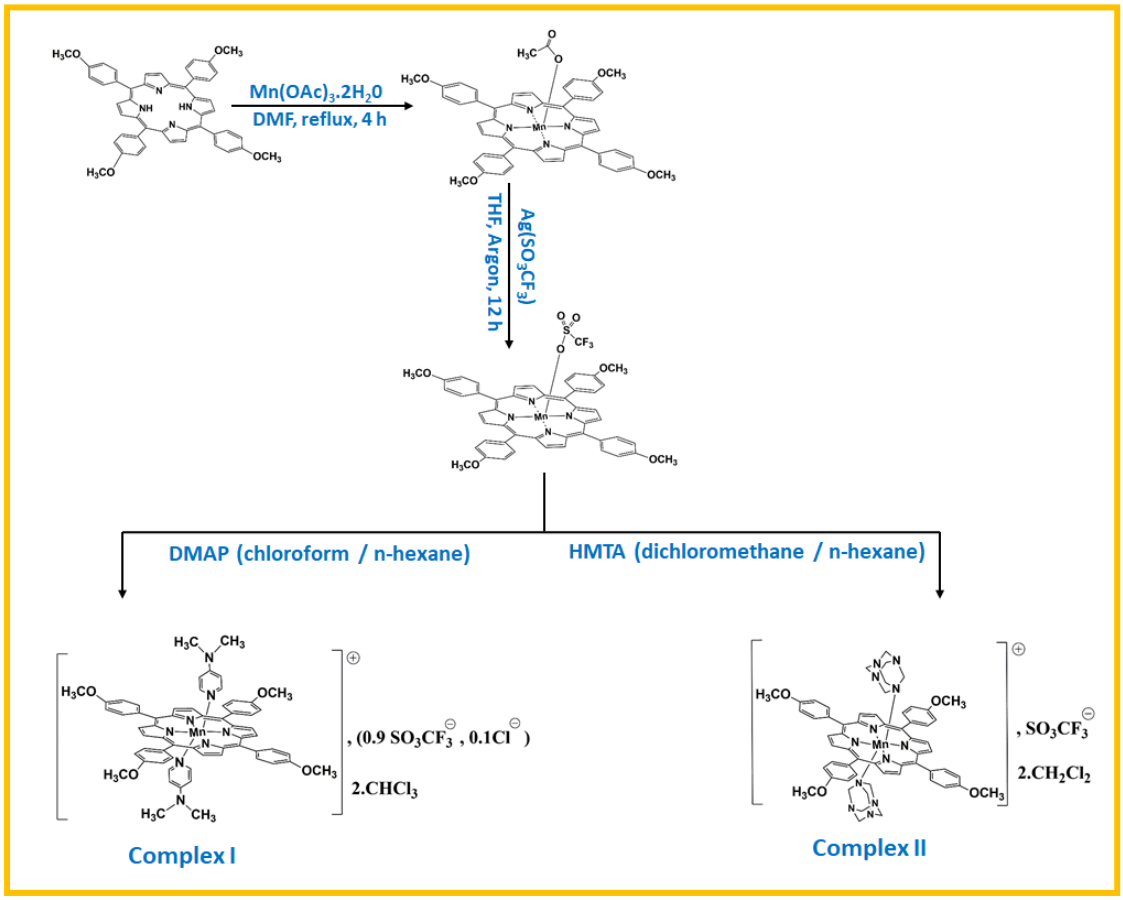

Scheme 1. Scheme of the synthesis of $[Mn^{III}(TMPP)(DMAP)_2](0.9SO_3CF_3)(0.1Cl)\cdot 2CHCl_3$ (**I**) and $[Mn^{III}(TMPP)(HMTA)_2](SO_3CF_3)\cdot 2CH_2Cl_2$ (**II**).

3-2. X-ray molecular structures of I-II

Complex **I** crystallized in the monoclinic crystal system with *P2₁/c* space group while complex **II** crystallized in the triclinic crystal system with *P-1* space group. The asymmetric unit of **I** is made by one $[Mn^{III}(TMPP)(DMAP)_2]^+$ ion complex, 0.9 $(SO_3CF_3)^-$ and 0.1Cl^- as counterions and two chloroform solvent molecules. For complex **II**, the asymmetric unit contains: one half $[Mn^{III}(TMPP)(HMTA)_2]^+$ ion complex, one half $(SO_3CF_3)^-$ counterion and one dichloromethane solvent molecule. Figure 1 illustrates the Ortep drawing of the $[Mn^{III}(TMPP)(DMAP)_2]^+$ ion complex while Figure 2 shows the Ortep diagram of the $[Mn^{III}(TMPP)(DMAP)_2]^+$ ion complex. The manganese polyhedral in complexes **I-II** are illustrated in Figures 3 and 4.

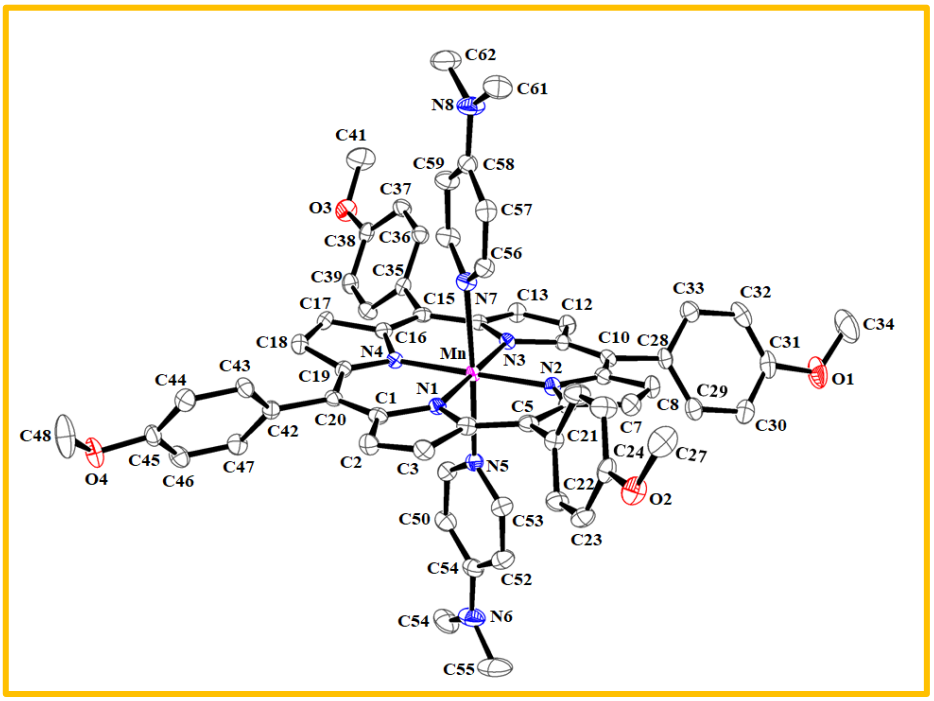

Fig. 1. ORTEP diagram of the $[Mn(TMPP)(DMAP)_2]^+$ ion complex (**I**) with thermal ellipsoids drawn at 40% probability. The hydrogen atoms are omitted for clarity.

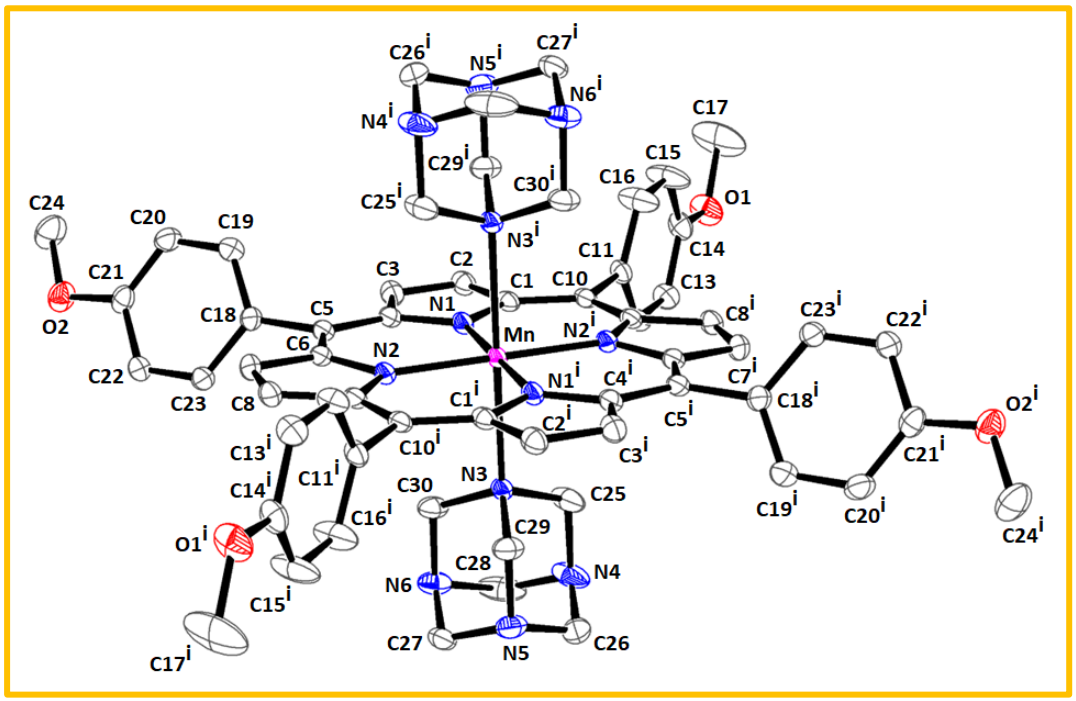

Fig. 2. ORTEP diagram the $[Mn(TMPP)(HMTA)_2]^+$ ion complex (**II**) with thermal ellipsoids drawn at 40% probability. The hydrogen atoms are omitted for clarity. Symmetry code (i): -x, -y, -z.

For **I**, the manganese(III) center ion is chelated by the four pyrrole nitrogen atoms of the TMPP porphyrinate and the two *trans* DMAP axial ligands (Figure 1). In the case of **II**, as shown by Figure 2, the Mn(III) center metal is chelated by the four pyrrole nitrogen atoms of the TMPP porphyrinate and the apical positions are occupied by two HMTA ligands. The two Mn—N(DMAP) bond lengths for **I** are 2.308(3) and 2.324(3) Å which are in the range [2.293 – 2.388] Å of the related Mn(III)-DMAP non-porphynic complexes (Table 3). In the case of **II**, the Mn—N(HMTA) distance is 2.439 (2) Å which is slightly higher than those of the related Mn(III)-HMTA non-porphyrinic complexes ranging between 2.194 and 2.342 Å (Table 3). It has been reported that pentacoordinated and hexacoordinated manganese(III) metalloporphyrins are high-spin (S = 2) with the $[(d_{xz}.d_{yz})^2.(d_{xy})^1.(d_{z^2})^1]$ ground state electronic configuration **[22,29]**. The mean equatorial distance between the Mn(III) cation and the four nitrogen atoms of the porphyrin macrocycle (Mn—Np) is 2.019(3) Å for **I** and 2.009(2) Å for **II**. These values are very close and in the [1.997(5) – 2.021(2)] Å range for Mn(III) metalloporphyrins (Table 3).

For the Mn(III)-TMPP-DMAP derivative (**I**), the dihedral angle (ϕ) between the pyridyl groups of the *trans* DMAP axial ligands is equal to zero (parallel orientation of these two cycles). For the same complex **I**, the values of the dihedral angles (φ) between the DMAP plane and the closest N(pyrrole)-Mn-N(DMAP) plane is 38° which is close to that of the related magnesium(II) [Mg(TClPP)(DMAP)$_2$] (TClPP = *meso*-tetra(*para*-chlorophenyl)porphyrinte) **[24]** with a φ value of 30° (Figure 5). Notably, the φ value in these Mn(III) and Mg(II) DMAP metalloporphyrins are quite close 45° which leads to a minimum nonbonded interaction between the porphyrin core atoms and the planar axial ligand hydrogen atoms **[30]**.

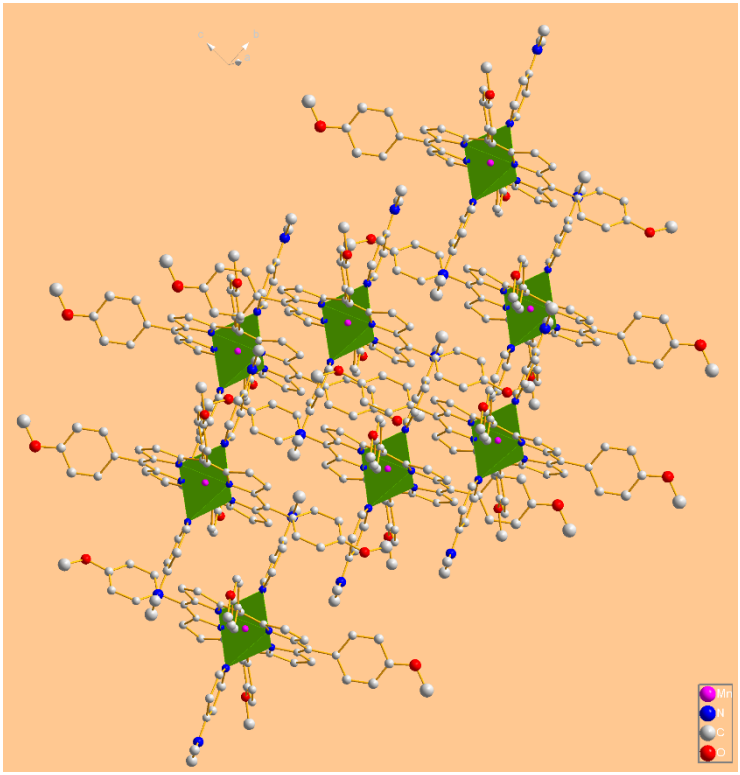

Fig. 3. View showing the manganese polyhedral in complex **I**.

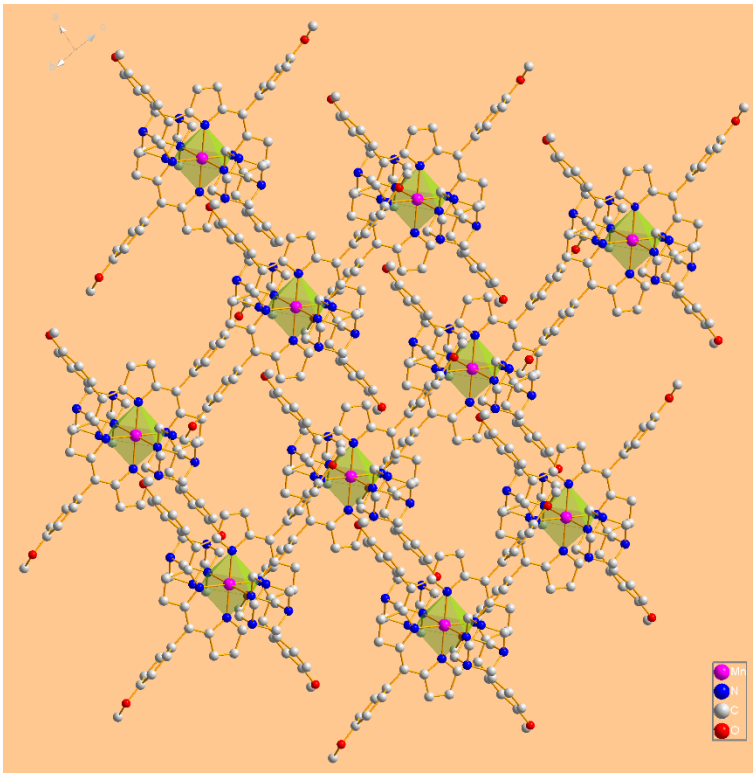

Fig. 4. View showing the manganese polyhedral in complex **II**.

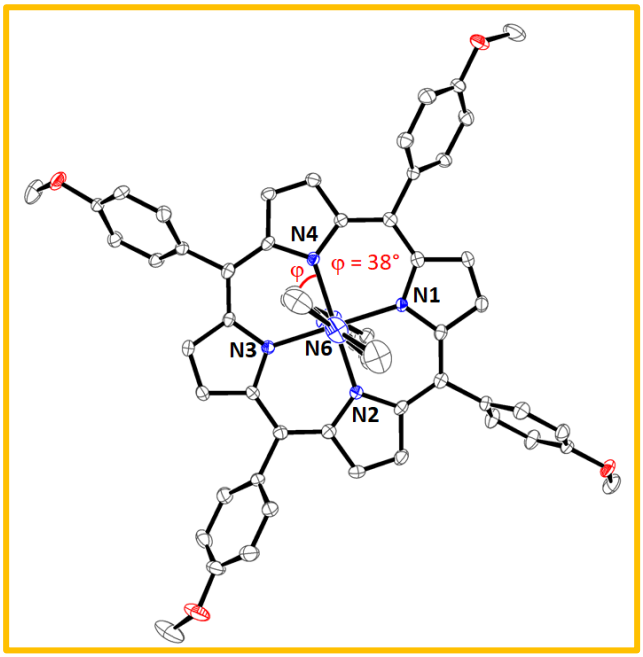

Fig. 5. Top view of the $[Mn^{III}(TMPP)(DMAP)_2]^+$ ion complex showing the orientation of the two *trans* DMAP axial ligands.

In Figure 6 is shown the formal diagrams of the porphyrin macrocycles of complexes **I-II** illustrating the displacements of each atom from the mean plane of the 24-atom porphyrin core in units of 0.01 Å. Inspection of this figure shows that the porphyrin core of the Mn(III)-Porph-HMTA derivative (**II**) is practically planar for which the maximum displacement value of an atom from the mean plane of the 24-atom porphyrin core is 0.08 Å. In contrast, the porphyrin macrocycle of the Mn(III)-Porph-DMAP derivative (**I**) exhibits important *ruffling* and *saddling* deformations. It should be recalled that a *ruffled* porphyrin macrocycle presents high values of the displacements of the *meso*-carbon atoms alternatively above and below the porphyrin core while the *saddle* deformation is due to the displacement of the pyrrole rings alternately above and below the mean porphyrin macrocycle **[31]**. The important deformation of the porphyrin macrocycle of complex **I** compared to that of complex **II** can only be due to the nature of the axial ligand since the same porphyrin (TMPP) is present for both complexes **I-II**. The two *trans* DMAP axial ligands coordinated to the Mn (III) cation in the case of complex **I** are spherically hindered due to the two methyl groups. In order to have the minimum interaction between the phenyl hydrogens of the TMPP porphyrin and those of the DMAP ligand, the porphyrin macrocycle of complex **I** undergoes a significant distortion, and the phenyls are no longer perpendicular to the mean plane of the porphyrin ring. Indeed, in the case of complex **II**, the dihedral angles between the porphyrin core and the phenyl groups are 88.28° and 61.81° while in case of complex **I**, these angles values are 75,96°, 75,76°, 58.19° and 57.94°.

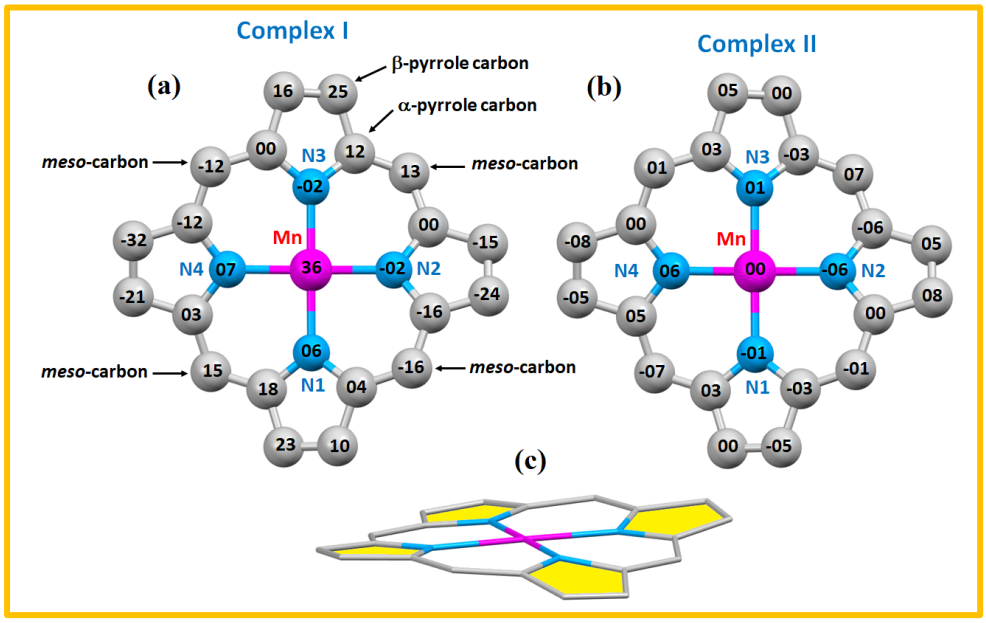

Fig. 6. Formal diagrams of the porphyrin macrocycles of **I-II**. **(a):** Complex **I**, **(b):** complex **II** and **(c):** Porphyrin core of **I** shown the *ruffling* and the *saddling* deformations. The displacements of each atom from the 24-atom core plane in units of 0.01 Å are illustrated.

The crystal packing of **I** is sustained by C—H···O, C—H…F, C—H···Cg (Cg = centroid of a pyrrole or pyridyl rings), C—F···Cg (Cg: centroid of a phenyl ring) and C—Cl···Cg (Cg = centroid of a pyridyl rings intermolecular interactions) involving the $[Mn^{III}(TMPP)(DMAP)_2]^+$ ion complex, the two chloroform solvents molecules (C64-Cl1-Cl2-Cl3 and C65-Cl4-Cl5-Cl-6) and the $(SO_3CF_3)^-$ counterion (Table S1, Figure 7, and Figures S5-S6-S7). For **II**, the crystal packing is made by C—H···O, C—H···N, C—H···Cl and C—H···Cg (Cg = centroid of a pyrrole ring) interactions involving the $[Mn^{III}(TMPP)(HMTA)_2]^+$ ion complex, the $(SO_3CF_3)^-$ counterion and the dichloromethane solvent molecules (Table S2, Figure 8 and Figure S8).

Table 3. Selected bond lengths [Å] and angles [°] for **I-II** and several porphyrinic and non-porphyrinic manganese(III) complexes.

Complex	$Mn–N_p$ [a]	$M–X_L$ [b]	ϕ [c]	φ [d]	Ref.
Manganese(III) meso-arylporphyrins					
$[Mn^{III}(TMPP)Cl]$	1.998(4)	2.365(1)	-	-	[18]
$[Mn^{III}(TPP)(CN)]$ [e]	2.009	2.1658	-	-	[32]
$[Mn^{III}(TPP)(2,6\text{-lutO})_2]C1O_4$ [e,f]	1.997(5)	2.262(4)/2.263(5)	-	-	[33]
$[Mn^{III}(TPP)(HIm)_2]Cl$ [e,g]	2.021(2)	2.285(2)/2.284(2)	38.0	12.4/12.6	[23]
$\{[Mn^{III}(TPP)(Him)_2]\}_n$ [e]	2.020/2.019	2.185/2.279	0	28.1/35.9	[34]
$\{[Mn^{III}(TPP)(4,4'\text{-bipy})_2]\}_n$ [e]	2.012/2.010	2.321/2.362	-	12.6/11.8	[35]
$[Mn^{III}(TClPP)(py)]^+$ [,i]	2.016(2)	2.216(3)	-	33.02	[36]

$[Mn^{III}(TPP)(pip)_2]$[e,j]	2.018(2)	2.370(2)	-	39.3	[23]
$[Mn^{III}(TPP)Cl(py)]$[e,k]	2.007(1)	2.420(1)/2.469(4)	-	30.7	[23]
$[Mn^{III}(TPP)Cl(DABCO)]$[e,l]	2.018(3)	2.612(3)/2.425(1)	-	-	[23]
$[Mn^{III}(TPP)(TCA)]$[e;m]	2.005(3)	2.053(3)	-	-	[22]
$[Mn^{III}(TBrPP)(TCA)]$[n,m]	2.008(4)	2.057(4)	-	-	[37]
$[Mn^{III}(TMPP)(DMAP)_2]^+$ **I**	2.019(3)	2.308(3)/2.324(3)	0	38.8:38.2	t.w.
$[Mn^{III}(TMPP)(HMTA)_2]^+$ **II**	2.009(2)	2.439(2)	-	-	t.w.
Non porphyrinc Manganese(III)-HMTA complexes					
$[Mn^{III}(O)(L_1)_6(HMTA)_3]$[o]	-	2.180/2.342/2.194	-	-	[38]
$\{[Mn^{III}(O)(L_1)_6(HMTA)_2]\}_n$[o]	-	2.187/2.180	-	-	[39]
Non porphyrinc Manganese(III)-DMAP complexes					
$[Mn^{III}(N_3)(L_2)(DMAP)]$[p]	-	2.388	-	-	[40]
$[Mn^{III}(Pc)(DMPA)_2]$[q]	-	2.293/2.307	-	-	[41]

[a]: M–Np = average equatorial manganese-nitrogen pyrrole distance, [b]: M–X_L = metal-axial ligand distance [c]: ϕ = the dihedral angle between the pyridyl groups of the DMAP axial ligand, [d]: φ = dihedral angles between the DMAP plane and the closest N(pyrrole)-Mn-N(DMAP) plane, [e]: TPP = *meso*-tetraphenylporphyrinate, [f]: 2,6-lutO = 2,6-Lutidine N-oxide, [g]: Him = imidazole, i: TClPP = *meso*-tetra(*para*-chlorophenyl)porphyrinate, [j]: pip = pipyridine, [k]: py = pyridine, [l]: DABCO = 1,4-diazabicyclo[2.2.2]octane, [m]: TCA = trichloroactetate, [n]: TBrPP = *meso*-tetra(*para*-bromophenyl)porphyrinate, o: L1 = pivalato-O,O', [p]: L2 = N,N'-bis(acetylacetone)-1,2-ethylenedi-iminato, [q]: Pc = phthalocyanine.

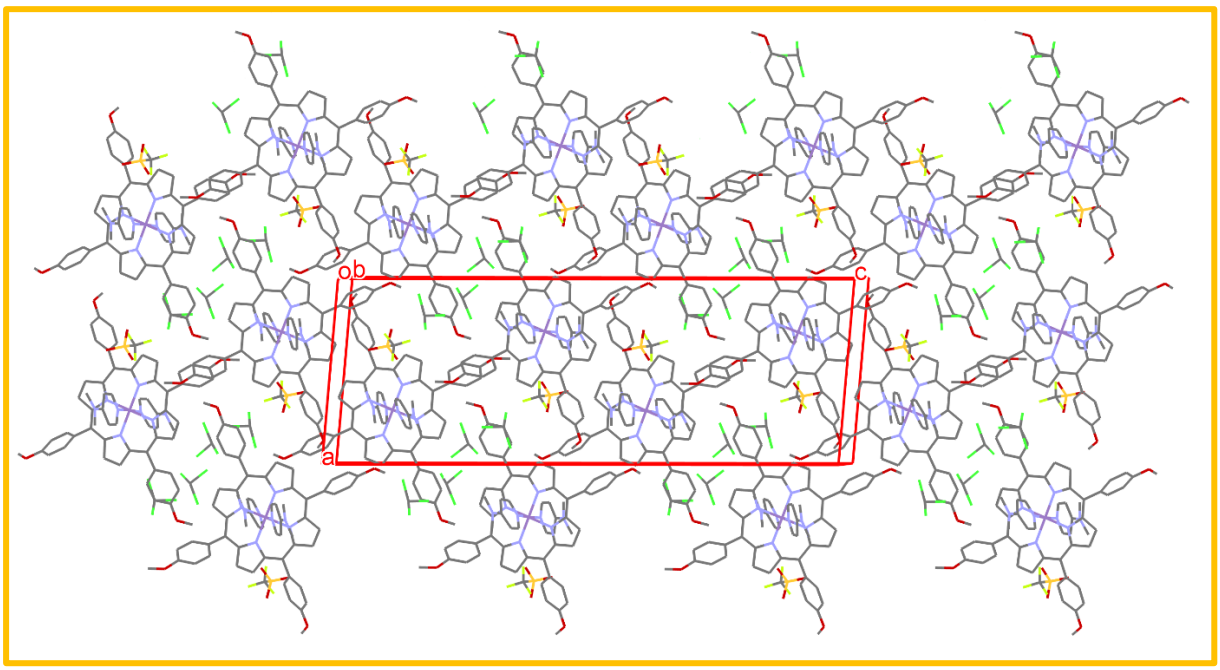

Fig. 7. View of the crystal lattice of **I** according to the [010] direction.

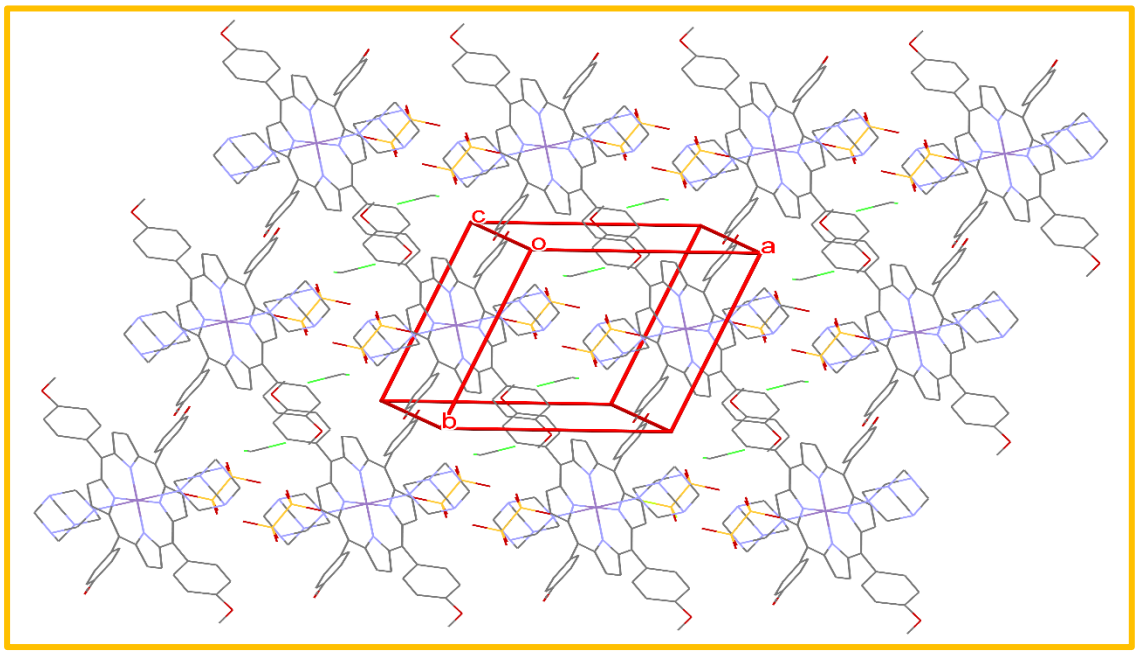

Fig. 8. View of the crystal lattice of **II** view along the [001] direction.

3.3. Hirshfeld Surface Analysis

Hirshfeld surface analysis is an invaluable tool for providing additional insight into intermolecular interactions in the packing of chemical species in crystals [42]. Hirshfeld surfaces and the two-dimensional fingerprint plots of our two synthetic Mn(III) porphyrin complexes (**I-II**) which are shown as transparent to allow visualization of the asymmetric unit of the given crystal structure, are illustrated in Figures 9 and 10, respectively. These Hirshfeld surfaces have been mapped over a d_{norm} range of -1.4978 Å to 1.7435 Å for **I** and from -0,1923 Å to 1,9321 Å for **II**.

Fingerprint plots for different types of intermolecular interactions for **I-II** are also depicted in Figure S11 and S12. The red shaded areas on the Hirshfeld surface indicate the presence of close contacts and areas without close contacts are shown in blue color. Hirshfeld surface analysis of complex **I** shows that the proportion of H…H interactions has the most significant contribution (39.9%) to the total Hirshfeld surface. For the same Mn(III)-TMPP-DMAP species (**I**), the other contributions are: H…C/C…H, H…O/O…H, H…Cl/Cl…H and H…F/F…H are 19.2%, 13.3%, 13% and 7.3%, respectively (Figures S11 and S13). For complex **II**, the most significant contribution is also H…H (46.4%) and the remain contributions are: H…F/F…H, H…C/C…H, H…Cl/Cl…H and H…O/O…H are 18.3%, 9.8%, 9.3% and 7.9%, respectively (Figures S12 and S13). These results are in concordance with those obtained by the PLATON program mentioned above.

The shape-index surface indicating a red concave region represents the acceptor atom while a blue convex region is indicative of a donor atom. As depicted in Figure S14-a, for **I** the presence of red area on several pyrrole and phenyl rings of the TMPP porphyrinate, the pyridyl group of the DMAP ligand and the triflate counterions indicate the existence of C—H···O and C—H···Cg (π) interactions. The blue area in the shape-index of **I**, are shown in the chloroform solvents and the counterion regions. In the case of **II**, the red convex areas are shown on the phenyl and pyrrole rings of the TMPP porphyrinate, the dichloromethane molecules and the triflate counterion which confirms the C—H···O, C—H···Cl; C—H···F and C—H···Cg intermolecular interactions given by the PLATON program. For the same complex **II**, the convex blue areas are located mostly around the HMTA axial ligand and the dichloromethane solvent molecules. As seen in Figure S14-b (curvedness surface) the absence of flat green regions separated by blue outline is indicative of the absence of π-π stacking intermolecular interaction for both complexes **I-II**.

3.4. UV/Vis spectroscopy

UV/Vis spectroscopic studies on high-spin Mn(III) porphyrin complexes have been extensively studied, especially the chloro-manganese(III)-tetraphenylporphyrin complex [Mn^{III}(TPP)Cl] **[43–45]**. These Mn(III) metalloporphyrins present hyper *d-type* electronic spectra with a half unoccupied *3d* metal orbitals with e_g symmetry [$d\pi$: d_{zx} and d_{yz}] (Figure 9) **[10]**. In the 360 – 420 nm region of the spectra of these complexes, two principal absorption bands named VI and Va are shown. The absorption bands known as bands V, QIV and QIII are shown between 470 and 700 nm (Figure 10). The QIII and QIV bands are attributed to the π → π* porphyrin transition between the HOM a_{2u} orbital to the e_g* LUMO orbital **[46]**. The band V known as the Soret band is attributed: *(i)* mostly to the porphyrin-Mn(III) charge transfer (LMCT) between the a_{1u}, a_{2u} porphyrin orbitals to the half occupied d_{zx} and d_{yz} ($d\pi$) orbitals of Mn(III) and *(ii)* to the classic π-π*: $a_{1u} \rightarrow e_g$* transition **[46]**. In the near UV region of the spectra, the absorption band VI is due to the electronic transition from the a_{2u} porphyrin orbital to the a_{1g} pure manganese d_{z^2} orbitals while the Va absorption band mostly derives from an $a_{2u} \rightarrow$ eg [$d\pi$: d_{zx} and d_{yz}] LMCT excitation **[46]** (Figure 9 and 10). It is noteworthy that the emplacement of the Soret band of manganese(III) porphyrin coordination compounds gives information about the oxidation state of the central metal and the spin state of these compounds **[43]**. Thus, the λ_{max} values of the Soret band of high-spin (S = 5/2) manganese(II) metalloporphyrins are between 437 and 445 nm. For high-spin (S = 2) Mn(III) porphyrins, the λ_{max} values are between 470 – 490 nm while low-spin Mn (III) metalloporphyrins present Soret band ~ 440 nm. For Mn(IV) and Mn(V) porphyrin complexes, λ_{max} values of the Soret band are at about 420 nm (Table 4). The UV/Vis spectra of our Mn(III) porphyrin derivatives **I-II** are depicted in Figure 10 and in Table 4 are summarized the UV/Vis data of several Mn(II), Mn(III), Mn(IV) and Mn(V) *meso*-arylporphyrins. The λ_{max}

values for **I-II** of the VI, Va, V, QIV and QIII absorption bands are 394, 410, **483**, 579, 617 and 396, 418, **488**, 588, 626 nm, respectively. The Soret bands at ~ 485 nm for **I-II** is an indication that these species are high-spin (S =2) Mn(III) porphyrin complexes. The Soret band λ_{max} value or the [Mn^{III}(TMPP)(SO_3CF_3)] which is 481 nm indicates that this species is also a high-spin Mn(III) porphyrin complex.

Table 4. UV/Vis data of complexes **I-II** and a selection of *meso*-arylporphyrins and manganese metalloporphyrins.

Complex	Oxidation State	Spin	Solvent	Soret Bands	Q Bands		Ref.
				λ_{max} (nm) (logε)			
$[Mn^{II}(TMP)]$[a]	II	5/2	CH_2Cl_2		437	-	[43]
$[Mn^{II}(TPP)]$[b]	II	5/2	DMSO		437	-	[43]
$[Mn^{II}(TpivPP)(2\text{-}MeHIm)]$[c,d]	II	5/2	THF		444	535, 573, 613	[47]
$[Mn^{II}(TPP)(DABCO)]$[b,e]	II	5/2	solid	340	453	526, 580, 619	[48]
$[Mn^{II}(TPP)(py)]$[b,f]	II	5/2	THF	-	440	532, 575, 613	[49]
$[Mn^{III}(TBrPP)(TCA)]$[g,i]	III	2	CH_2Cl_2	380, 403	474	575, 610	[22]
$[Mn^{III}(TPP(H_2O)](SO_3CF_3)$[a]	III	2	$CHCl_3$	386	474	570, 604	[50]
$[Mn^{III}(TPP)Cl]$[b]	III	2	$CHCl_3$	376	476	581, 617, 690	[45]
$[Mn^{III}(TPP)(NO_2)]$[b]	III	2	Benzene	380, 400	476	583, 620	[51]
$[Mn^{III}(TPP)(HIm)_2]Cl$[b,j]	III	2	$CHCl_3$	-	478	-	[23]
$[Mn^{III}(TPP)(py)_2]Cl$[b,f]	III	2	Pyridine	380	476	578, 613, 690	[45]
$[Mn^{III}(TMPP)(OAc)]$	III	2	CH_2Cl_2	382(5.98), 407(5.96), 482(6.08)		586(5.42), 624(5.44)	t.w.
$[Mn^{III}(TMPP)(SO_3CF_3)]$	III	2	CH_2Cl_2	394(6.09), 410(6.06), 481(6.08)		577(5.53), 614(5.56)	t.w.
$[Mn^{III}(TMPP)(DMAP)_2]$ **(I)**	III	2	CH_2Cl_2	394(6.02), 410(5.99), 483(6.05)		579(5.40), 617(5.45)	t.w.
$[Mn^{III}(TMPP)(HTMA)_2]$ **(II)**	III	2	CH_2Cl_2	396(6.08), 418(6.03), 488(6.05)		588(5.53), 626(5.62)	t.w.
$K[Mn^{III}(TPP)(CN)_2]$[b]	III	1	DMSO	-	435	545, 668	[52]
$K[Mn^{III}(TPP)(Im)_2]$[b,k]	III	1	DMSO	-	435	545, 668	[52]
$[Mn^{IV}(TMP)(OCH_3)_2]$[a]	IV	3/2	Acetonitrile	-	422	-	[52]
$[Mn^{IV}(TMP)(O)]$[a]	IV	3/2	CH_2Cl_2		422	-	[52]
$[Mn^{V}(TPP)(N)]$[b]	V	-	Chlorobenzene		424	-	[51]

a: TMP = *meso*-tetramesitylporphyrinate, b: TPP = *meso*-tetraphenylporphyrinate, c: TpivPP = α,α,α,α-tetrakis(*o*-pivalamidophenyl) porphinate, d: 2-MeHIm = 2-methylimidazole, e: DABCO = 1,4-diazabicyclo[2.2.2]octane, f: py = pyridine, g: TBrPP = *meso*-tetra(*para*-bromophenyl)porphyrinate, i: TCA = trichloroacetate, j: Him = imidarole, k: Im = imidazolate.

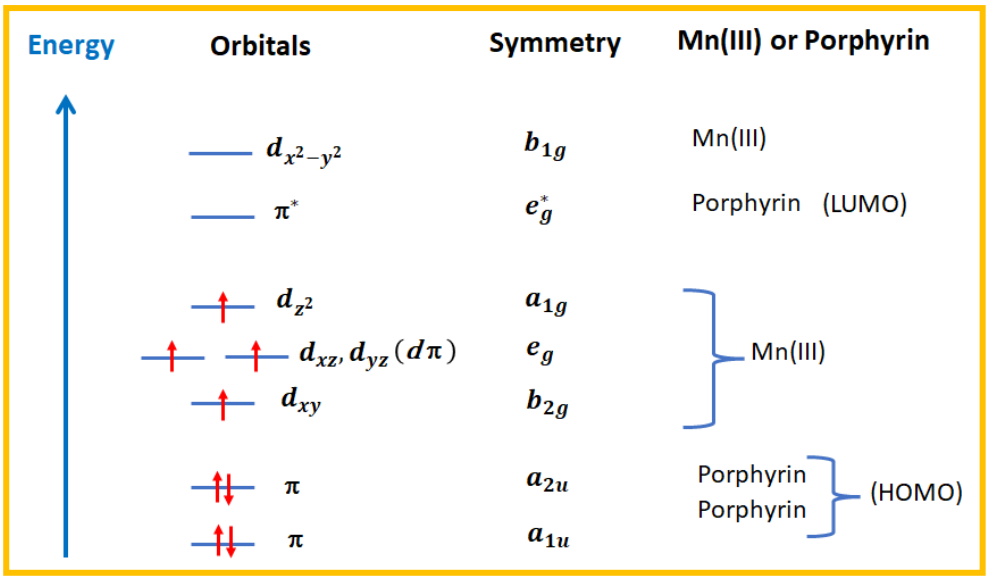

Fig. 9. Diagram showing the energy levels of the d orbitals of Mn(III) of high-spin (S = 2) metalloporphyrins and those of the HOMO and LUMO orbitals of the porphyrin [10].

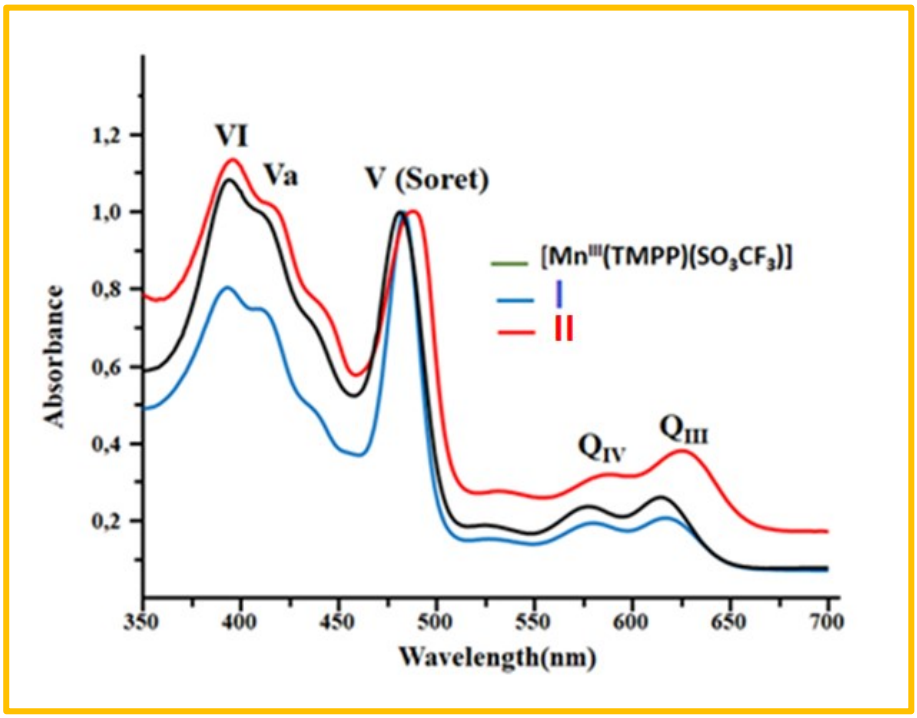

Fig. 10. Electronic absorption spectra of $[Mn^{III}(TMPP)(SO_3CF_3)]$ and **I-II** at ca. 10^{-6} M in dichloromethane.

3.5. Cyclic voltammetry investigation

Electrochemical studies on Mn(III) metalloporphyrins started in the early sixties [53] and since 1982, Kadish *et al.,* published many cyclic voltammetry investigations on these $3d^4$ transition metal porphyrin coordination compounds [54–57]. The chloro-Mn(III) tetraphenylporphyrin complex was the most studied $[Mn^{III}(Porph)X]$ type compounds (Porh = *meso*-artlporphyrin and X is an anionic

halogen or pseudo-halogen axial ligand) (Table 5). For these pentacoordinated Mn(III) complexes, the voltammograms include: *(i)* two reversible one electron oxidation waves attributed to the oxidation of the porphyrin core, *(ii)* one electron reversible wave corresponding to the Mn(III)/Mn(II) reduction and *(iii)* two reduction waves attributed to the reductions of the porphyrin macrocycle **[58]**. The cyclic voltammogram of our [Mn^{III}(TMPP)(SO_3CF_3)] starting material is illustrated in Figure S15 while those of complexes **I-II** are depicted in Figure 11. The electrochemical data of these three porphyrinic species as well as those of several Mn(III) metalloporphyrins are summarized in Table 5. It is noteworthy that the voltammograms of our Mn(III)-DMAP-TMPP and Mn(III)-HMTA-TMPP (**I-II**) species are the first examples of voltammograms of [Mn^{III}(Porph)$(L)_2$]$^+$ type ion complexes (L = neutral axial ligand) and all the reported ones refer to pentaccordinated Mn(III) metalloporphyrins type [Mn^{III}(Porph)X] (X = ionic axial ligand). The half potential values of the first and second oxidation waves [(O1,R1 and (O2,R2)]) for **I-II** are 1.11/1.09, 1.53/1.40 V, the $E_{1/2}$ of the Mn(III)/Mn(II) reduction wave (R3,O3) of **I-II** are -0.24 and -0.15 V, respectively. The $E_{1/2}$ values of the first (R4,O4) and second (R5,O5) reduction waves for **I-II** are -1.48/-1.49 and -1.57/ -1.89 V, respectively. For **II**, we noticed the presence of a third irreversible wave (O6) which could be attributed to the third oxidation of the porphyrin ring. An inspection of the data in Table 5 revels that the cyclic voltammograms of **I-II** resemble to those of the reported [Mn^{III}(Porph)X] complexes and the $E_{1/2}$ values of the different waves are very close to those to these pentaccortdinated Mn(III) derivatives. We also notice that the $E_{1/2}$ potential value of the Mn(III)/Mn(II) reduction (-0.15 V) of complex **II** is more shifted toward negative values that that of complex **I** and the other Mn(III) metalloporphyrins reported in Table 5 except of [Mn^{III}(TPP)(OH)] for which the half wave potential of the Mn(III)/Mn(II) reduction is -0.13 V. This indicates that complex **II** is easier to reduce than complex **I**.

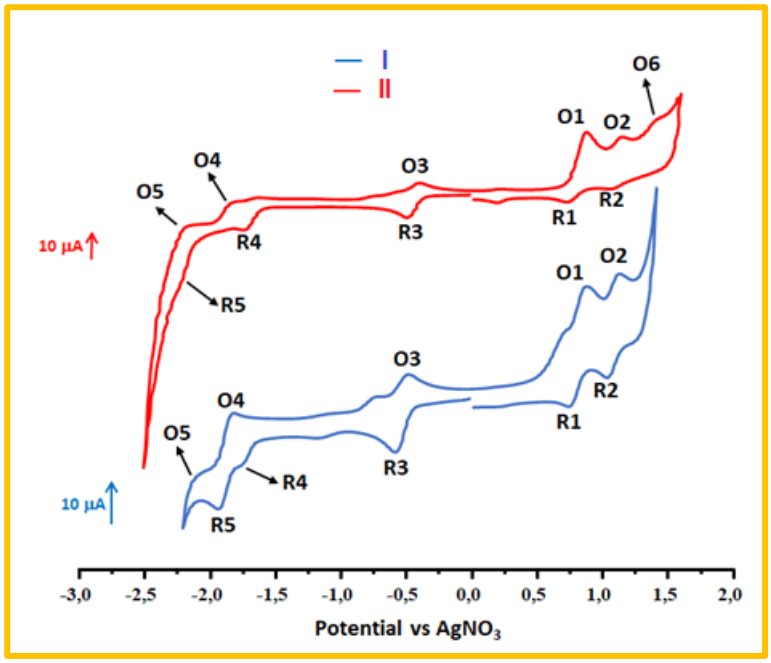

Fig. 11. Cyclic voltammograms of **I** and **II**. The solvent used is the dichloromethane, and the concentration is ca. 10^{-3} M in 0.2 M TBAP, 50 mV/s, vitreous carbon working electrode (Ø = 3 mm).

Table 5. Electrochemical data[a] for $[Mn^{III}(TMPP)(SO_3CF_3)]$, complexes **I-II** and a selection of Mn(III) *meso*-metalloporphyrins.

	Solvent	**Oxidations**		**Reductions**			**Ref.**
		1st Porph Oxid (O1,R1) $E_{1/2}$[b]	2nd Porph Oxid (O2,R2) $E_{1/2}$	Mn(III)/Mn(II) red. (R3,O3) $E_{1/2}$	1nd Porph Red (R4,O4) $E_{1/2}$	2nd Porph Red (R5,O5) $E_{1/2}$	
$[Mn^{III}(TPP)Cl]$[c]	CH_2Cl_2	1.14	-	-0.29	-1.52	-	[54]
$[Mn^{III}(TPP)Cl]$[c]	benzonitrile	1.28	1.64	-0.24	-1.31	-1.80	[56]
$[Mn^{III}(TPP)(N_3)]$[c]	CH_2Cl_2	1.18	-	-0.34	-1.52	-	[54]
$[Mn^{III}(TPP)I]$[c]	CH_2Cl_2	-	-	-0.24	-	-	[54]
$[Mn^{III}(TPP)(ClO_4)]$[c]	CH_2Cl_2	1.28	1.64	-0.21	-1.47	-1.79	[56]
$[Mn^{III}(TPP)(NCS)]$[c]	CH_2Cl_2	1.19	-	-0.25	-1.57	-	[54]
$[Mn^{III}(TPP)(OH)]$[c]	CH_3CN	1.34	1.60	-0.13	-1.43	-	[58]
$[Mn^{III}(TPP)(TCA)]$[c,d]	CH_2Cl_2	1.34	1.58	-0.33	-1.48*	-1.70	[22]
$[Mn^{III}(TBrPP)(TCA)]$[e,d]	CH_2Cl_2	1.24	1.56	-0.38	-1.49	-1.70*	[22]
$[Mn^{III}(TMPP)(SO_3CF_3]$	CH_2Cl_2	1.08	1.37	-0.39	-1.60	-1.93*	this work
$[Mn^{III}(TMPP)(DMAP)_2]^+$ (**I**)	CH_2Cl_2	1.11	1.53	-0.24	-1.48	-1.57	this work
$[Mn^{III}(TMPP)(HMTA)_2]$ (**II**)	CH_2Cl_2	1.09	1.40	-0.15	-1.49	-1.89	this work

[a]: Potentials are reported versus SCE, [b] : $E_{1/2}$ = half wave potential, c: TPP = *meso*-phenylporphyrinate, [d]: TCA = trichloroacetate, [e]: TBrPP = *meso*-tetra(*para*-bromophenyl)porphyrinate, *: irreversible wave.

3.6. Biological Studies

3.6.1. Antibacterial screening

Porphyrins, both natural and artificial, have relatively low toxic effects *in vitro* and *in vivo*. They are used inter alia for their potential biological activities because of their ability to (*i*) stimulate peroxidase and oxidase reactions [59], (*ii*) absorb photons, (*iii*) produce reactive oxygen species (ROS) [60], and (*iv*) be partially localized through bacterial membrane lipid. Porphyrins form a class of compounds with prominent potential as new factors and procedures versus pathogenic microorganisms due to their great molecular engineering capability and a lot of different mechanisms by which they affect microbial and viral pathogens. In the present work, the *in vitro* antibacterial action of the H_2TMPP free base porphyrin, the [Mn^{III}(TMPP)(SO_3CF_3)] starting materials and complexes **I-II** were tested against two strains of Gram-positive (*S. aureus* (ATCC 25923) and *B. cereus* (ATCC 14579)) and two strains of Gram-negative (*P. aeruginosa* (ATCC 27853) and *E. coli* (ATCC 35218)) by the well agar diffusion screening method mentioned by Mahdhi *et al.* [61]. The antibacterial efficacy of these synthesized compounds was tested *in vitro* towards a number of pathogenic bacteria and compared to that of the two standard antibiotics, ampicillin and tetracycline [62,63]. Figure 12 exhibits the diameters of inhibition regions found using the diffusion assay.

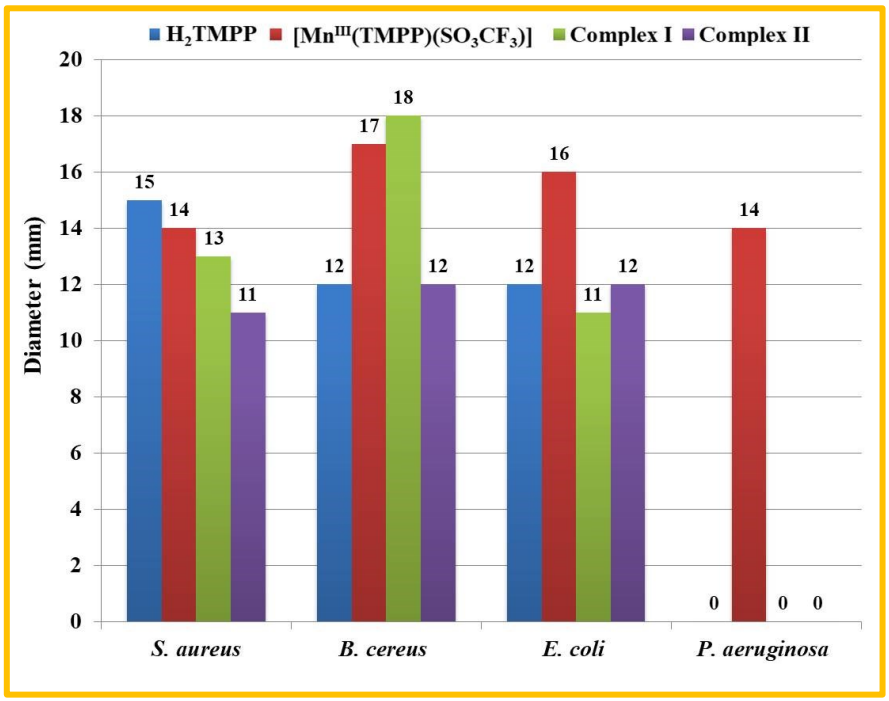

Fig. 12. *In vitro* antibacterial activity of H_2TMPP, [Mn^{III}(TMPP)(SO_3CF_3)] and **I-II**.

All compounds displayed activity against most strains and the data revealed that the strains Gram-positive (*S. aureus* and *B. cereus*) were the most sensitive compared to the gram-negative bacteria (*P. aeruginosa* and *E. coli*) (Figure 12). The difference in sensitivity between both bacteria types against porphyrin derivatives is probably caused by differences in cell membrane structure. Gram negative bacteria have an

outer membrane while gram-positive bacteria do not [64] The presence of an outer membrane causes foreign molecules to be unable to diffuse easily through the cell wall. According to the findings of the inhibition zones, the H_2TMPP free base porphyrin was not active against *P. aeruginosa* and showed less antibacterial activity against *E. coli* and *B. cereus* with an inhibition zone of 12 mm. The presence of manganese in the porphyrinic core also affects the antibacterial activity. The [Mn^{III}(TMPP)(SO_3CF_3)] complex shows a zone inhibition diameter of 14 mm against *S. aureus* and *P. aeruginosa*. It also inhibited *E. coli* (16 mm) and *B. cereus* (17 mm). On the other hand, the addition of the DMAP and HTMA axial ligands to the triflate-Mn(III)-TMPP derivative (leading to **I-II**, respectively), slightly weakens the antibacterial activity around 11 mm, except for the strain *B. cereus*, for which it exhibits a higher inhibition zone around 18 mm. These values are also close to the standard drug tetracycline, which shows a diameter ~12 mm of inhibition zone vs *P. aeruginosa* and *E. coli* **[62]**, but remain lower than the standard antibiotic ampicillin, which owns 22 and 30 mm in diameter of zone inhibition against *B. cereus* and *E. coli*, respectively [63]. According to the literature, the antibacterial activity of our compounds remains lower compared to the non-porphyrinic synthesized compounds. For instance, Alswat *et al.* [65–67], synthesized Zeolite based materials and investigated their antibacterial properties and according to the results, their nanocomposites produced diameters of zones of inhibition between 24 and 28 mm against *E. coli* E266. Notably, our findings are similar to those obtained for other metalloporphyrins such as [Mg(TPBP)] and [M(TPP)] (TPBP = *meso*-(tetrakis-[4-(benzoyloxy)phenyl] porphyrinate, TPP = *meso*-tetraphenylporphyrinate, M = Fe(II), Ni(II), Cu(II), Zn(II) and Pt(II)) [68,69], where the activities are equivalent to or much than those of the H_2TMPP free base porphyrin. The increased activity of the Mn(III)-complexes, with respect to the corresponding H_2TMPP free porphyrin, can be explained on the basis of Overtone's concept and Tweedy's Chelation theory [70,71]. According to Overtone's concept of cell permeability, the lipid membrane that surrounds the cell favors the passage of only the lipid soluble materials as the liposolubility is an important factor which controls the activity. The chelation of the metal ion decreases its polarity to a greater extent due to the overlap of the ligand orbital. Moreover, it increases the delocalization of the π-electrons over the whole chelated ring and enhances the lipophilicity of the complexes. This increased lipophilicity enhances the penetration of the complexes into the lipid membrane and restricts further multiplicity of the microorganisms.

3.6.2. Antifungal activity

The antifungal activities of our four porphyrinic compounds present non attendance of inhibition zones which were quantitatively evaluated towards three yeast strains (*C. krusei ATCC6258*, *C. albicans ATCC90028* and *C. neoformans ATCC14116*) and three strains of fungal (*A. flavus 15UA005*, *A. niger 15UA006* and *A. fumigatus ATCC204305*). Figure 13 depicts the diameters of inhibition regions defined using the diffusion assay.

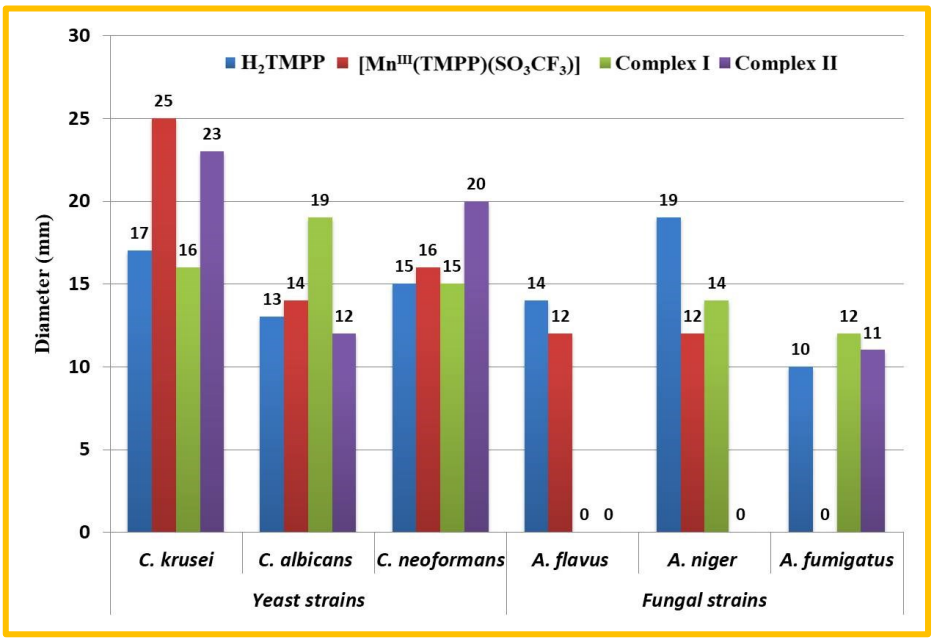

Fig. 13. *In vitro* antifungal activity of H_2TMPP, [Mn^{III}(TMPP)(SO_3CF_3)] and **I-II**.

It has been reported that porphyrin derivatives have potent antifungal properties [72,73]. Overall, the current investigation clearly indicates that the three yeast strains have a superior reactivity compared to those of the three fungi strains and that the yeast straining *C. krusei* is the most sensitive. For yeasts strains, it is concluded that *(i)* the antifungal activity of the free base porphyrin increases upon coordination of Mn(III) and *(ii)* [Mn^{III}(TMPP)(SO_3CF_3)] inhibited the growth of fungi more than the unmetalled porphyrin under identical experimental conditions (Figure 13). This complex has shown 25 mm in diameter of zone inhibition against *C. krusei*, 14 mm in diameter of zone inhibition against *C. albicans* and 16 mm against *C. neoformans*. On the contrary, the H_2TMPP free base porphyrin presents a higher inhibitory effect on the growth of fungi (between 10 and 19 mm) than the manganese(III) metalloporphyrin. Furthermore, for complexes **I** and **II**, the coordination of the two N-donor axial ligands DMAP and HTMA displayed lower inhibition zones, and in some cases even superior, to the starting products. These manganese porphyrinic coordination compounds showed a zone inhibition diameter between 16 and 23 mm and of 15 to 20 mm against *C. krusei* and *C. neoformans*, respectively. They also inhibited *A. niger* (12 - 14 mm) and were not active against *A. flavus*. These complexes exhibit less antifungal activity than the standard drug Nystatin [74], which possessed a zone of inhibition at 29 mm against *C. albicans* and 19 mm against *A. fumigatus*. According to the review of the literature, the antifungal efficacies of the manganese complexes are analogous while in some circumstances are slightly greater to previously synthesized and studied metalloporphyrins. For example, Singh *et al.* [74], synthesized several new *meso*-arylporphyrins complexes [Metal ion = Cu(II), Co(II), Ni(II)] and investigated their antifungal properties. These porphyrinic complexes produced diameters of zones of inhibition between 15 mm and 22 mm against *C. albicans* and between 10 mm and 19 mm against *A. fumigatus*. Moreover, our complexes are slightly more active than

Mn(III) and Co(II)-based porphyrin derivatives reported by Karimipour *et al.,* (*A. fumigatus* between 9 mm and 11 mm) [75] but remain in the same principles explaining the activity increase for the metal complexes [76,77]. Depending on the rule of overtone for cellular permeability [76,77] and due to the lipophilicity as an important factor in controlling the antifungal efficacy, the lipid membrane that surrounds the cell, allows only lipid-soluble materials to pass in. According to the Tweet's chelation theory [78], the metal ion's polarity would be diminished to a greater degree because of the overlap of the porphyrin orbital and the partial sharing of the metal ion's positive charge with the donor groups. As a result, the polarity of Mn-porphyrin compounds is reduced, and their liposolubility is greatly increased. Metalloporphyrin's penetration into lipid membranes is reinforced by this rise in lipophilicity which disturbs the cell's respiration process.

3.6.3. Antioxidant activity

To test antioxidant activity and describe how antioxidant agents function, several antioxidant methods and modifications have been suggested. The most used methods for determining the radical scavenging ability of various samples are the 2,2-diphenyl-1-picrylhydrazyl (DPPH) and the 2,2'-azino-bis(3-ethylbenzothiazoline-6-sulphonic acid) (ABTS) radical assay. DPPH and ABTS radicals are related with known inflammatory results and have been often used to investigate the potential antioxidant activity of compounds [79] which may also bear a potential anticancer and anti-inflammatory activity [80]. *In vitro*, the capacity of H_2TMPP, [Mn^{III}(TMPP)(SO_3CF_3)], and complexes **I-II** to scavenge DPPH, ABTS was assessed to compare with that of the vitamin C as a reference composite (Figures 14 and 15).

3.6.3.1. DPPH free radical scavenging activity

The quite stable DPPH nitrogen-centered radical possesses a absorption property that decreases with exposure to antioxidants [81]. It reacts with hydrogen donating function leading a color shift from purple to yellow. The intensity of this phenomenon is related to the number of electrons captured [82], i.e., the further the free radical scavenging capability of an antioxidant composite, the more DPPH is reduced, and the sample becomes less purple in color. The scavenging activities of our four porphyrinic compounds were evaluated against DPPH. IC50 values were surveyed, and the percentage values of the antioxidant activity were given in Figure 14.

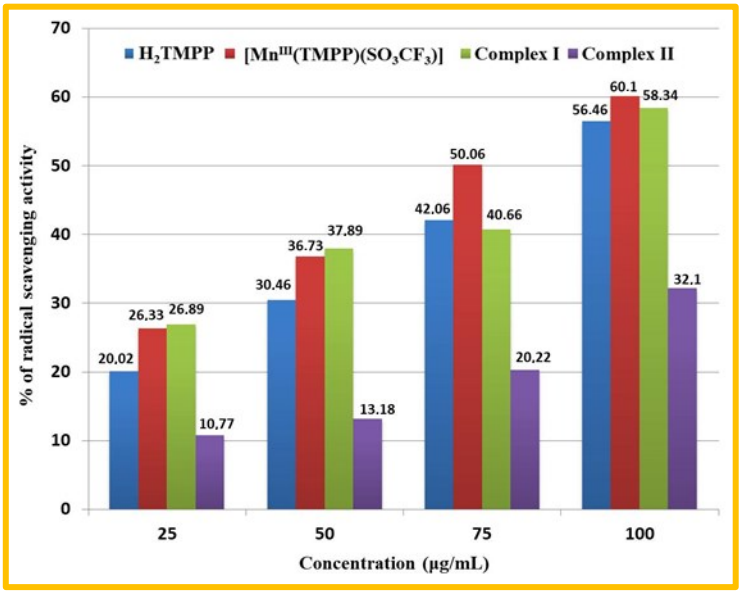

Fig. 14. Emission DPPH radical scavenging activity of H_2TMPP, [Mn^{III}(TMPP)(SO_3CF_3)] and **I-II**.

The free radical scavenging activity of our four porphyrinic compounds is concentration dependent. The rate of the free radical scavenging heightened as the composite solution concentration increases. With the increasing concentration of the compounds, the free radicals of DPPH decrease and tend to stabilize. In higher concentrations, the highest antioxidant activity was obtained for [Mn^{III}(TMPP)(SO_3CF_3)] and complex **I** with respect to complex **II** (Figure 14). By comparison with the H_2TMPP free base porphyrin, these Mn-metalloporphyrins show slightly higher antioxidant activity. Specifically, at 100 µg/mL and 75 µg/mL they present antioxidant potential between 40% and 60%, with the same concentrations which are much superior to complex **II** (32% at 100 µg/mL). By comparison with the already well-known antioxidants, our synthetic species are slightly less active in the same range of concentrations. As far as radical scavenging activity is concerned and at a concentration of 100 µg/mL, the vitamin C (Vit C), the Butylated Hydroxy-Toluene (BHT) and the Epigallocatechin gallate (EGCG) for example reach approximatively 70 and 80% [83–85]. The results of the radical scavenging were also expressed in terms of half-inhibition concentration (IC50) which denotes the concentration required to scavenge 50% of DPPH radicals, such as the higher IC50 values representing lower antioxidant activity. The results we obtained are as follows: 88.56 µg/mL for H_2TMPP, 74.91 µg/mL for [Mn^{III}(TMPP)(SO_3CF_3)], 85.7 µg/mL for complex **I**, and >100 µg/mL for complex **II**. According to these IC50 values, the [Mn^{III}(TMPP)(SO_3CF_3)] starting material and complex **I** show high activity and display close IC50 values and are slightly higher than that of the H_2TMPP free-base porphyrin. On the contrary, the lowest activity is observed for complex **II** (>100 µg/mL). In comparison with their analogs, our studied compounds are more active against DPPH than the free ligands and even against other transition metal complexes [86–90]. The obtained results for our porphyrinic species are in accordance with the fact that upon the coordination of a center ion, the antioxidant activity increases slightly. This could be explained by the additional radical scavenging by the

metal center leading to the increase the ability of the porphyrinic species to scavenge free radicals by stabilizing the unpaired electrons.

As already inspected and mentioned in the literature [91], the radical scavenging activity (and related prevention of oxidative damage) is correlated to the standard reduction potential of the species, i.e. the lower the value of the standard reduction potential of a compound, the better its electron donor character is, which means that the compound exhibits stronger antioxidant properties. Complex **II** displayed the highest value of reduction potential as compared to our other tested compounds. This indicates also, that this species exhibits the weakest antioxidant activity.

The ABTS cation which has a blue color and absorbs light at 734 nm is reactive toward most known antioxidant compounds capable of giving a hydrogen atom or an electron such as vitamin C, thiols and phenolics. During the reaction, the color of the ABTS radical cation changes from blue to colorless corresponding to its neutral form. In Figure 15 is shown the ABTS radical scavenging activities of the H_2TMPP free-base porphyrin, [Mn^{III}(TMPP)(SO_3CF_3)] and complexes **I-II**.

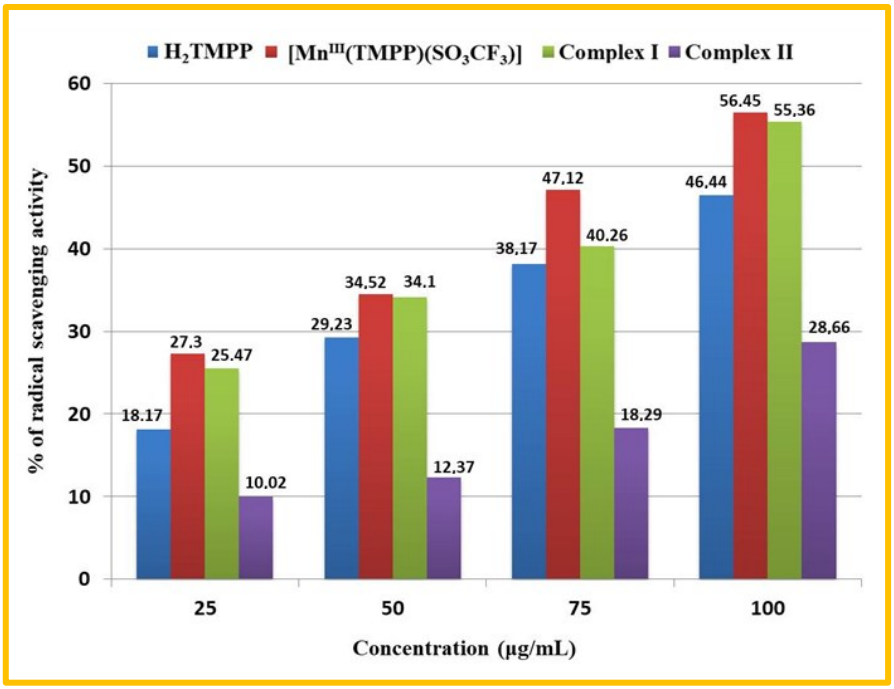

Fig. 15. Emission ABTS radical scavenging activity of H_2TMPP, [Mn^{III}(TMPP)(SO_3CF_3)] and **I-II**.

As expected, free radical scavenging activity of our porphyrinic compounds is concentration dependent. The results revealed that all compounds possess an inhibitory effect on ABTS+, and the highest antioxidant activity was obtained for [Mn^{III}(TMPP)(SO_3CF_3)]. Moreover, the values were significantly increased with increasing concentrations. [Mn^{III}(TMPP)(SO_3CF_3)] ion presents 27.3% ABTS radical formation inhibition at 25 µg/mL which increases with increasing concentration to attain 56.45% at 100 µg/mL. Complex **I** exhibit similar antioxidant activity with 55.36% ABTS radical formation inhibition, at 100 µg/mL. On the other hand, complex **II** shows much lower activity (28.66 at 100 µg/mL) compared to the other tested

compounds and this difference could be attributed to the two DMAP axial ligands coordinated to Mn(III). This also may be responsible for the higher antioxidant activity of this species, since it has a dimethylamine group which is an important factor for the increase of the antioxidant activity [92]. Our four compounds exhibit lower antioxidant activity than the standard vitamin C [87]. Moreover, and according to the literature, our compounds exhibit lower antioxidant activity than those obtained with the *meso*-tetrakis[4-(benzoyloxy)phenyl] porphyrin metallated by Co(II) (78% ABTS radical formation inhibition) [83]. Under the reaction conditions used in our case, the IC50 value of H_2TMPP is 90.49 µg/mL, while the IC50 values for H_2TMPP, [Mn^{III}(TMPP)(SO_3CF_3)] and the complexes **I-II** are 77.11, 87.31, 90.49 and >100 µg/mL, respectively. The RSA percentages can be classified in the following order: [Mn^{III}(TMPP)(SO_3CF_3)] > complex **I** > H_2TMPP > complex **II**.

As a conclusion, the antioxidant activity results of the H_2TMPP free-base porphyrin and its corresponding manganese complexes against the free radicals DPPH˙ and ABTS˙+ show that the [Mn^{III}(TMPP)(SO_3CF_3)] displays higher scavenging activity than the H_2TMPP free-base porphyrin and complex **II**, with decreasing order as follows: [Mn^{III}(TMPP)(SO_3CF_3)] > complex **I** > H_2TMPP > complex **II**. On the other hand, the antioxidant activity of the Mn(III) complexes against the DPPH˙ radical are better than that against the ABTS˙+ radical.

As the manganese(III) metalloporphyrin shows stronger radical scavenging activity towards DPPH˙ than towards ABTS˙+ radical, the scavenging mechanism of DPPH˙ by [Mn^{III}(TMPP)(SO_3CF_3)] was chosen to be studied in detail. The DPPH˙ is characterized by two absorbances at 331 and 518 nm by UV/Vis. We noticed that as the concentration of [Mn^{III}(TMPP)(SO_3CF_3)] increases, the intensities of the two absorption bands at 331 and 518 nm decrease to disappear completely while a new band located at 428 nm appears (Figure 16). The 428 nm absorption band are maximized at 90 µg/mL then decreased upon increasing the concentration of the Mn(III)-triflate complex to 105 or 120 µg/mL (Figure 16) due to the exchange of the anion form of DPPH− to DPPH-H [93]. This observation could be an indication of the presence of DPPH• in the reaction leading to the DPPH- anion form [94]. This UV/Vis study indicates the two steps mechanism for the scavenging reaction of DPPH by [Mn^{III}(TMPP)(SO_3CF_3)] complex involving an electron transfer followed by a proton transfer. The result agrees with those obtained using other coordination compounds [93,95].

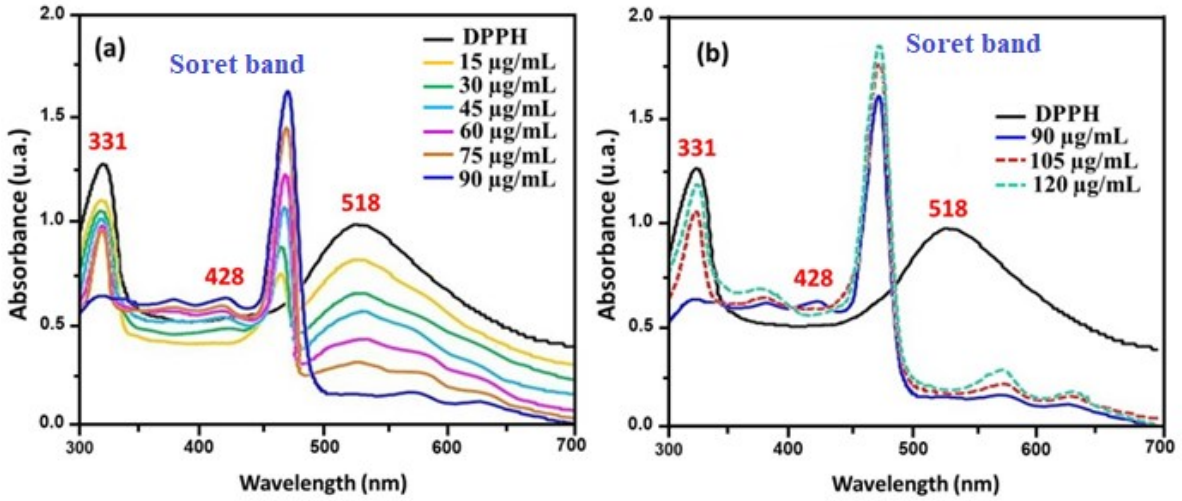

Fig. 16. UV/Vis spectra monitoring the reaction between DPPH and [Mn^{III}(TMPP)(SO_3CF_3)].
(a): ranging 15–90 µg/mL and **(b):** ranging 90–120 µg/mL.

4. Conclusion

In the present work we have synthesized the bis(4-dimethylaminopyridine) and the bis(hexamethylenetetramine) manganese(III) ions complexes with the *meso*-tetra(*para*-methoxyphenyl)porphyrin (**I-II**). These species were characterized by UV/Vis and IR spectroscopies and elemental analysis. The hyper *d-type* electronic spectrum of **I-II** with a redshifted Soret band at ~ 488 nm is an indication that these Mn(III) metalloporphyrins are high spin (S =2) complexes. The cyclic voltammetry (CV) investigation on **I-II** are the first examples of voltammograms of $[Mn^{III}(Porph)(L)_2]^+$ type ion complexes (L = neutral axial ligand). The CV data for **I-II** present two reversible one electron oxidation waves attributed to the oxidation of the porphyrin core, one electron reversible wave corresponding to the Mn(III)/Mn(II) reduction and two reduction waves attributed to reductions of the porphyrin macrocycle. These physicochemical studies of complexes **I-II** show that the Mn(III) ion and the porphyrinic ring are the major responsible of the electronic properties of Mn(III) metalloporphyrins and that the substituted groups at the *para*-phenyl positions of the *meso*-aryporphyrins as well as the nature of the axial ligands have practically no role on the electronic properties of this type of Mn(III) complexes. The molecular structures of **I-II** were determined by single crystal X-ray diffraction. The supramolecular assemblies in the crystal of these two Mn(III) derivatives are assumed by non-classic C—H···C, C—H···O, C—H···N, C—H···Cg, C—Cl···Cg and C—F···Cg (Cg are the centroids of pyrrole and phenyl rings) intermolecular contacts. These intermolecular interactions were confirmed by Hirshfeld surface analysis.
The antibacterial efficacy of the H_2TMPP free base porphyrin, the [Mn^{III}(TMPP)(SO_3CF_3)] starting material, and **I-II** were tested *in vitro* towards several pathogenic bacteria and compared to that of the

typical antibiotic tetracycline. These four porphyrinic species present quite different antibacterial inhibition properties but close to the standard tetracycline drug. The antifungal activities of our four porphyrinic species were evaluated towards three yeast strains and three strains of fungal. The antifungal activities of these synthetic compounds differ from one entity to another and from one strain to another but overall, the results obtained are encouraging. Furthermore, the *in vitro* capacity of the H_2TMPP free-base porphyrin, [Mn^{III}(TMPP)(SO_3CF_3)] and complexes **I-II** to scavenge DPPH and ABTS was tested. These investigations revealed that the most active derivatives were [Mn^{III}(TMPP)(SO_3CF_3)] and complex **I**.

Supporting information

Supplementary data associated with this article can be found, in the online version, at Complete crystallographic data for the structural analysis have been deposited with the Cambridge Crystallographic Data Centre; CCDC reference numbers 2144173 and 2165563. These data can be obtained free of charge via www.ccdc.cam.ac.uk/conts/retrieving.html (or from the Cambridge Crystallographic Data Centre, 12 Union Road, Cambridge CB2 1EZ, UK; fax: (+44) 1223 336033; e-mail: deposit@ccdc.cam.uk).http://xxxxxxxxxxxxxxxxxxxxxxxxx.

Notes

The authors declare no competing financial interest.

Acknowledgements

The authors gratefully acknowledge financial support from the Ministry of Higher Education and Scientific Research of Tunisia. The author would like to express their gratitude to Prince Sattam Bin Abdulaziz University, Al-Kharj, Saudi Arabia for providing administrative and technical support.

References

[1] R. Willstätter, A. Stoll, Untersuchungen über Chlorophyll: Methoden und Ergebnisse, Springer-Verlag, 2013.

[2] R. Tschesche, Die Chemie des Pyrrols. Von H. Fischer u. H. Orth. II. Band: Pyrrolfarbstoffe. 1. Hälfte: Porphyrine – Hämin – Bilirubin und ihre Abkömmlinge. 764 Seiten. Akademische Verlagsgesellschaft m. b. H., Leipzig 1937. Preis geh. RM. 42, —, geb. RM. 44, —, Angew. Chem. 51 (1938) 27–27. https://doi.org/10.1002/ange.19380510110.

[3] A.D. Adler, F.R. Longo, J.D. Finarelli, J. Goldmacher, J. Assour, L. Korsakoff, A simplified synthesis for meso-tetraphenylporphine, J. Org. Chem. 32 (1967) 476–476. https://doi.org/10.1021/jo01288a053.

[4] J.L. Sessler, E. Tomat, Transition-Metal Complexes of Expanded Porphyrins, Acc. Chem. Res. 40 (2007) 371–379. https://doi.org/10.1021/ar600006n.

[5] J. Barona-Castaño, C. Carmona-Vargas, T. Brocksom, K. de Oliveira, Porphyrins as Catalysts in Scalable Organic Reactions, Molecules. 21 (2016) 310. https://doi.org/10.3390/molecules21030310.
[6] Z. Liang, H.-Y. Wang, H. Zheng, W. Zhang, R. Cao, Porphyrin-based frameworks for oxygen electrocatalysis and catalytic reduction of carbon dioxide, Chem. Soc. Rev. 50 (2021) 2540–2581. https://doi.org/10.1039/D0CS01482F.
[7] X. Jiang, Z. Zhou, H. Yang, C. Shan, H. Yu, L. Wojtas, M. Zhang, Z. Mao, M. Wang, P.J. Stang, Self-Assembly of Porphyrin-Containing Metalla-Assemblies and Cancer Photodynamic Therapy, Inorg. Chem. 59 (2020) 7380–7388. https://doi.org/10.1021/acs.inorgchem.9b02775.
[8] J. Tian, B. Huang, M.H. Nawaz, W. Zhang, Recent advances of multi-dimensional porphyrin-based functional materials in photodynamic therapy, Coordination Chemistry Reviews. 420 (2020) 213410. https://doi.org/10.1016/j.ccr.2020.213410.
[9] L.J. Boucher, Manganese porphyrin complexes. I. Synthesis and spectroscopy of manganese(III) protoporphyrin IX dimethyl ester halides, J. Am. Chem. Soc. 90 (1968) 6640–6645. https://doi.org/10.1021/ja01026a014.
[10] L.J. Boucher, Manganese porphyrin complexes. III. Spectroscopy of chloroaquo complexes of several porphyrins, J. Am. Chem. Soc. 92 (1970) 2725–2730. https://doi.org/10.1021/ja00712a024.
[11] C.J. Weschler, B.M. Hoffman, F. Basolo, Synthetic oxygen carrier. Dioxygen adduct of a manganese porphyrin, J. Am. Chem. Soc. 97 (1975) 5278–5280. https://doi.org/10.1021/ja00851a043.
[12] E.B. Fleischer, J.M. Palmer, T.S. Srivastava, A. Chatterjee, Thermodyamic and kinetic properties of an iron-porphyrin system, J. Am. Chem. Soc. 93 (1971) 3162–3167. https://doi.org/10.1021/ja00742a012.
[13] J.M. Olson, The Evolution of Photosynthesis, Science. 168 (1970) 438–446. https://doi.org/10.1126/science.168.3930.438.
[14] L.K. Hanson, Axial ligand effects on iron and manganese porphyrins: Extended hückel calculations of cyt p450 analogs and of O2 binding to iron and manganese, International Journal of Quantum Chemistry. 16 (1979) 73–87. https://doi.org/10.1002/qua.560160705.
[15] J.T. Groves, W.J. Kruper, R.C. Haushalter, Hydrocarbon oxidations with oxometalloporphinates. Isolation and reactions of a (porphinato)manganese(V) complex, J. Am. Chem. Soc. 102 (1980) 6375–6377. https://doi.org/10.1021/ja00540a050.
[16] G. Li, A.K. Dilger, P.T. Cheng, W.R. Ewing, J.T. Groves, Selective C−H Halogenation with a Highly Fluorinated Manganese Porphyrin, Angew. Chem. 130 (2018) 1265–1269. https://doi.org/10.1002/ange.201710676.
[17] L.-Q. Mo, X.-F. Huang, G.-C. Wang, G. Huang, P. Liu, Full use of factors promoting catalytic performance of chitosan supported manganese porphyrin, Sci Rep. 10 (2020) 14132. https://doi.org/10.1038/s41598-020-70210-y.
[18] C.R. Groom, I.J. Bruno, M.P. Lightfoot, S.C. Ward, The Cambridge Structural Database, Acta Crystallogr B Struct Sci Cryst Eng Mater. 72 (2016) 171–179. https://doi.org/10.1107/S2052520616003954.
[19] S.L. Tong, J. Zhang, Y. Yan, S. Hu, J. Yu, L. Yu, Supramolecular assembly based on a series of meso-tetrakis(p-methoxyphenyl)porphrin complexes, Solid State Sciences. 13 (2011) 1320–1327. https://doi.org/10.1016/j.solidstatesciences.2011.03.029.
[20] P. Turner, M.J. Gunter, B.W. Skelton, A.H. White, Crystal Structures of the Pentacoordinate Bromo, Isocyanato, Iodo, Acetato and Isothiocyanato Complexes of the meso-Tetraphenylporphyrinatomanganese Cation, Aust. J. Chem. 51 (1998) 835. https://doi.org/10.1071/C97150.
[21] K.S. Suslick, R.A. Watson, Photochemical reduction of nitrate and nitrite by manganese and iron porphyrins, Inorg. Chem. 30 (1991) 912–919. https://doi.org/10.1021/ic00005a009.
[22] W. Harhouri, S. Dhifaoui, Z. Denden, T. Roisnel, F. Blanchard, H. Nasri, Synthesis, spectroscopic characterizations, cyclic voltammetry investigation and molecular structure of the high-spin manganese(III) trichloroacetato meso -tetraphenylporphyrin and meso -tetra-(para -

bromophenyl)porphyrin complexes, Polyhedron. 130 (2017) 127–135. https://doi.org/10.1016/j.poly.2017.04.008.
[23] N. Lahanas, P. Kucheryavy, R.A. Lalancette, J.V. Lockard, Crystallographic identification of a series of manganese porphyrin complexes with nitrogenous bases, Acta Crystallogr C Struct Chem. 75 (2019) 304–312. https://doi.org/10.1107/S2053229619001232.
[24] T. Fradi, O. Noureddine, F.B. Taheur, M. Guergueb, S. Nasri, N. Amiri, A. Almahri, T. Roisnel, V. Guerineau, N. Issoui, H. Nasri, New DMAP meso-arylporphyrin Magnesium(II) complex. Spectroscopic, Cyclic voltammetry and X-ray molecular structure characterization. DFT, DOS and MEP calculations and Antioxidant and Antifungal activities, Journal of Molecular Structure. 1236 (2021) 130299. https://doi.org/10.1016/j.molstruc.2021.130299.
[25] M.V. Tesakova, V.I. Parfenyuk, The Electrochemical Evaluation of the Antioxidant Activity of Substituted Tetraphenylporphyrins, Russ J Electrochem. 53 (2017) 1281–1285. https://doi.org/10.1134/S1023193517110155.
[26] N. Amiri, M. Hajji, F.B. Taheur, S. Chevreux, T. Roisnel, G. Lemercier, H. Nasri, Two novel magnesium(II) meso-tetraphenylporphyrin-based coordination complexes: Syntheses, combined experimental and theoretical structures elucidation, spectroscopy, photophysical properties and antibacterial activity, Journal of Solid State Chemistry. 258 (2018) 477–484. https://doi.org/10.1016/j.jssc.2017.11.018.
[27] N. Amiri, F.B. Taheur, S. Chevreux, E. Wenger, G. Lemercier, H. Nasri, Synthesis, crystal structure and spectroscopic characterizations of porphyrin-based Mg(II) complexes – Potential application as antibacterial agent, Tetrahedron. 73 (2017) 7011–7016. https://doi.org/10.1016/j.tet.2017.10.029.
[28] A. Bruker, Instrument Service v4. 2.7, APEX2, SADABS, SAINT-Plus & XPREP, (2014).
[29] The Porphyrins. Structure and Synthesis, Part A | David Dolphin (Eds.) | download, (n.d.). https://b-ok.africa/book/2217542/8e3b8d?dsource=recommend (accessed April 7, 2022).
[30] W.R. Scheidt, D.K. Geiger, R.G. Hayes, G. Lang, Control of spin state in (porphinato)iron(III) complexes. An axial ligand orientation effect leading to an intermediate-spin complex. Molecular structure and physical characterization of the monoclinic form of bis(3-chloropyridine)(octaethylporphinato)iron(III) perchlorate, J. Am. Chem. Soc. 105 (1983) 2625–2632. https://doi.org/10.1021/ja00347a018.
[31] C.J. Kingsbury, M.O. Senge, The shape of porphyrins, Coordination Chemistry Reviews. 431 (2021) 213760. https://doi.org/10.1016/j.ccr.2020.213760.
[32] W.R. Scheidt, Y.J. Lee, W. Luangdilok, K.J. Haller, K. Anzai, K. Hatano, Preparation and molecular stereochemistry of metalloporphyrin complexes with cyano ligands. Cyano(pyridine)(meso-tetraphenylporphinato)iron(III) hydrate and cyano(meso-tetraphenylporphinato)manganese(III) chloroform solvate, Inorg. Chem. 22 (1983) 1516–1522. https://doi.org/10.1021/ic00152a019.
[33] C.L. Hill, M.W. Williamson, Electronic and structural properties of a reactive metalloporphyrin with N-oxide axial ligands. Crystal and molecular structure of bis(2,6-lutidine N-oxide)(tetraphenylporphinato)manganese(III) perchlorate, Inorg. Chem. 24 (1985) 3024–3030. https://doi.org/10.1021/ic00213a031.
[34] J.T. Landrum, K. Hatano, W.R. Scheidt, C.A. Reed, Imidazolate complexes of iron and manganese tetraphenylporphyrins, J. Am. Chem. Soc. 102 (1980) 6729–6735. https://doi.org/10.1021/ja00542a011.
[35] R.K. Kumar, I. Goldberg, Crystal engineering with tetraarylporphyrins, an exceptionally versatile building block for the design of multidimensional supramolecular structures, Chem. Commun. (1998) 1435–1436. https://doi.org/10.1039/A802549E.
[36] D.K. Rittenberg, K. Sugiura, A.M. Arif, Y. Sakata, C.D. Incarvito, A.L. Rheingold, J.S. Miller, Products from the Reaction of meso-Tetrakis(4-halophenyl)porphinato-manganese(II) and Hexacyanobutadiene (HCBD): Formation of π-[HCBD]22− Dimers, μ-[HCBD].−, σ-[HCBD].−, and [C4(CN)5O]−, Chemistry – A European Journal. 6 (2000) 1811–1819. https://doi.org/10.1002/(SICI)1521-3765(20000515)6:10<1811::AID-CHEM1811>3.0.CO;2-6.
[37] W. Harhouri, S. Dhifaoui, Z. Denden, T. Roisnel, F. Blanchard, H. Nasri, Synthesis, spectroscopic characterizations, cyclic voltammetry investigation and molecular structure of the high-spin manganese(III) trichloroacetato meso -tetraphenylporphyrin and meso -tetra-(para -

bromophenyl)porphyrin complexes, Polyhedron. 130 (2017) 127–135. https://doi.org/10.1016/j.poly.2017.04.008.
[38] G.M. Dulcevscaia, I.G. Filippova, M. Speldrich, J. van Leusen, V.Ch. Kravtsov, S.G. Baca, P. Kögerler, S.-X. Liu, S. Decurtins, Cluster-Based Networks: 1D and 2D Coordination Polymers Based on {MnFe2(μ3-O)}-Type Clusters, Inorg. Chem. 51 (2012) 5110–5117. https://doi.org/10.1021/ic202644t.
[39] S.G. Baca, I.L. Malaestean, T.D. Keene, H. Adams, M.D. Ward, J. Hauser, A. Neels, S. Decurtins, One-Dimensional Manganese Coordination Polymers Composed of Polynuclear Cluster Blocks and Polypyridyl Linkers: Structures and Properties, Inorg. Chem. 47 (2008) 11108–11119. https://doi.org/10.1021/ic8014145.
[40] D.J. Darensbourg, E.B. Frantz, Manganese(III) Schiff Base Complexes: Chemistry Relevant to the Copolymerization of Epoxides and Carbon Dioxide, Inorg. Chem. 46 (2007) 5967–5978. https://doi.org/10.1021/ic7003968.
[41] D. McKearney, W. Zhou, C. Zellman, V.E. Williams, D.B. Leznoff, Facile tuning of strong near-IR absorption wavelengths in manganese(III) phthalocyanines *via* axial ligand exchange, Chem. Commun. 55 (2019) 6696–6699. https://doi.org/10.1039/C9CC02151E.
[42] M.A. Spackman, D. Jayatilaka, Hirshfeld surface analysis, CrystEngComm. 11 (2009) 19–32. https://doi.org/10.1039/B818330A.
[43] R.D. Arasasingham, T.C. Bruice, Reaction of hydroxide ion with manganese(III) tetramesitylporphyrin and the oxidation states of manganese tetramesitylporphyrins, Inorg. Chem. 29 (1990) 1422–1427. https://doi.org/10.1021/ic00332a028.
[44] I. Creanga, A. Palade, A. Lascu, M. Birdeanu, G. Fagadar-Cosma, E. Fagadar-Cosma, Manganese (III) porphyrin sensitive to H2O2 detection, Digest Journal of Nanomaterials and Biostructures. 10 (2015) 315–321.
[45] R.R. Gaughan, D.F. Shriver, L.J. Boucher, Resonance raman spectra of manganese (III) tetraphenylporphin halides., Proc. Natl. Acad. Sci. U.S.A. 72 (1975) 433–436. https://doi.org/10.1073/pnas.72.2.433.
[46] M.A. Fodor, P. Szabó, G. Lendvay, O. Horváth, Characterization of the UV-Visible absorption spectra of manganese(III) porphyrins with time-dependent density functional theory calculations, Zeitschrift Für Physikalische Chemie. 236 (2022) 27–51. https://doi.org/10.1515/zpch-2020-1787.
[47] Q. Yu, Y. Liu, D. Liu, J. Li, Geometric and electronic structures of five-coordinate manganese(II) "picket fence" porphyrin complexes, Dalton Trans. 44 (2015) 9382–9390. https://doi.org/10.1039/C5DT00685F.
[48] D.V. Konarev, S.S. Khasanov, A. Otsuka, G. Saito, R.N. Lyubovskaya, Formation of Antiferromagnetically Coupled C60•- and Diamagnetic (C70-)2 Dimers in Ionic Complexes of Fullerenes with (MDABCO+)2·MIITPP (M = Zn, Co, Mn, and Fe) Assemblies, Inorg. Chem. 46 (2007) 2261–2271. https://doi.org/10.1021/ic0611138.
[49] C.A. Reed, J.K. Kouba, C.J. Grimes, S.K. Cheung, Manganese(II) and chromium(II) porphyrin complexes: synthesis and characterization, Inorg. Chem. 17 (1978) 2666–2670. https://doi.org/10.1021/ic50187a057.
[50] W. Harhouri, C. Mchiri, S. Najmudin, C. Bonifácio, H. Nasri, Synthesis, FT–IR characterization and crystal structure of aqua(5,10,15,20-tetraphenylporphyrinato-κ ^{4} *N*)manganese(III) trifluoromethanesulfonate, Acta Crystallogr E Cryst Commun. 72 (2016) 720–723. https://doi.org/10.1107/S2056989016006630.
[51] C.L. Hill, F.J. Hollander, Structural characterization of a complex of Manganese(V) nitrido[tetrakis(p-methoxyphenyl)porphinato] manganese(V), J. Am. Chem. Soc. 104 (1982) 7318–7319. https://doi.org/10.1021/ja00389a072.
[52] A.P. Hansen, H.M. Goff, Low-spin manganese(III) porphyrin imidazolate and cyanide complexes. Modulation of magnetic anisotropy by axial ligation, Inorg. Chem. 23 (1984) 4519–4525. https://doi.org/10.1021/ic00194a023.
[53] P.A. Loach, M. Calvin, Oxidation States of Manganese Hematoporphyrin IX in Aqueous Solution *, Biochemistry. 2 (1963) 361–371. https://doi.org/10.1021/bi00902a032.

[54] S.L. Kelly, K.M. Kadish, Counterion and solvent effects on the electrode reactions of manganese porphyrins, Inorg. Chem. 21 (1982) 3631–3639. https://doi.org/10.1021/ic00140a010.
[55] R. Guilard, K. Perié, J.-M. Barbe, D.J. Nurco, K.M. Smith, E. Van Caemelbecke, K.M. Kadish, Electrochemical and Spectroscopic Characterization of Manganese(III) Dodecaphenylporphyrin Derivatives and X-ray Structural Determination of Chloro(5,10,15,20-tetrakis(pentafluorophenyl)-2,3,7,8,12,13,17,18-octaphenylporphyrinato)- manganese(III). Formation of a Manganese(IV) Species by Ozone and Electrochemical Oxidation, Inorg. Chem. 37 (1998) 973–981. https://doi.org/10.1021/ic970717w.
[56] M. Autret, Z. Ou, A. Antonini, T. Boschi, P. Tagliatesta, K.M. Kadish, Synthesis and electrochemistry of 2,3,7,8,12,13,17,18-octachloro-5,10,15,20-tetrakis (3,5-dichloro-2,6-dimethoxyphenyl)porphyrin (H2tdcdmpp), [CoII(tdcdmpp)] and [M(tdcdmpp)Cl](M = FeIII or MnIII), J. Chem. Soc., Dalton Trans. (1996) 2793–2797. https://doi.org/10.1039/DT9960002793.
[57] X. Jiang, C.P. Gros, Y. Chang, N. Desbois, L. Zeng, Y. Cui, K.M. Kadish, Tetracationic and Tetraanionic Manganese Porphyrins: Electrochemical and Spectroelectrochemical Characterization, Inorg. Chem. 56 (2017) 8045–8057. https://doi.org/10.1021/acs.inorgchem.7b00732.
[58] C.-H. Chang, S.-H. Cheng, Y. Oliver Su, Axial Ligand Effects on the Redox Reactions of Manganese Porphyrins, Jnl Chinese Chemical Soc. 46 (1999) 221–227. https://doi.org/10.1002/jccs.199900035.
[59] X. Wang, K. Qu, B. Xu, J. Ren, X. Qu, Multicolor luminescent carbon nanoparticles: Synthesis, supramolecular assembly with porphyrin, intrinsic peroxidase-like catalytic activity and applications, Nano Res. 4 (2011) 908–920. https://doi.org/10.1007/s12274-011-0147-4.
[60] U. Giri, M. Iqbal, M. Athar, Porphyrin-mediated photosensitization has a weak tumor promotingactivity in mouse skin: possible role of in situ-generatedreactive oxygen species, Carcinogenesis. 17 (1996) 2023–2028. https://doi.org/10.1093/carcin/17.9.2023.
[61] A. Mahdhi, M.Á. Esteban, Z. Hmila, K. Bekir, F. Kamoun, A. Bakhrouf, B. Krifi, Survival and retention of the probiotic properties of Bacillus sp. strains under marine stress starvation conditions and their potential use as a probiotic in Artemia culture, Research in Veterinary Science. 93 (2012) 1151–1159. https://doi.org/10.1016/j.rvsc.2012.05.005.
[62] F.R. Kooriyaden, S. Sujatha, C. Arunkumar, Study of scrambling in porphyrin forming reactions: Synthesis, structure, photophysical, electrochemical and antimicrobial studies, Polyhedron. 128 (2017) 85–94. https://doi.org/10.1016/j.poly.2017.03.002.
[63] F.B. Biswas, T.G. Roy, Md.A. Rahman, T.B. Emran, An in vitro antibacterial and antifungal effects of cadmium(II) complexes of hexamethyltetraazacyclotetradecadiene and isomers of its saturated analogue, Asian Pacific Journal of Tropical Medicine. 7 (2014) S534–S539. https://doi.org/10.1016/S1995-7645(14)60286-8.
[64] J.C. Lopez-Romero, H. González-Ríos, A. Borges, M. Simões, Antibacterial Effects and Mode of Action of Selected Essential Oils Components against *Escherichia coli* and *Staphylococcus aureus*, Evidence-Based Complementary and Alternative Medicine. 2015 (2015) 1–9. https://doi.org/10.1155/2015/795435.
[65] A.A. Alswat, M.B. Ahmad, T.A. Saleh, M.Z.B. Hussein, N.A. Ibrahim, Effect of zinc oxide amounts on the properties and antibacterial activities of zeolite/zinc oxide nanocomposite, Materials Science and Engineering: C. 68 (2016) 505–511. https://doi.org/10.1016/j.msec.2016.06.028.
[66] A.A. Alswat, M.B. Ahmad, T.A. Saleh, Preparation and Characterization of Zeolite\Zinc Oxide-Copper Oxide Nanocomposite: Antibacterial Activities, Colloid and Interface Science Communications. 16 (2017) 19–24. https://doi.org/10.1016/j.colcom.2016.12.003.
[67] A.A. Alswat, M.B. Ahmad, M.Z. Hussein, N.A. Ibrahim, T.A. Saleh, Copper oxide nanoparticles-loaded zeolite and its characteristics and antibacterial activities, Journal of Materials Science & Technology. 33 (2017) 889–896. https://doi.org/10.1016/j.jmst.2017.03.015.
[68] N. Amiri, M. Hajji, F.B. Taheur, S. Chevreux, T. Roisnel, G. Lemercier, H. Nasri, Two novel magnesium(II) meso-tetraphenylporphyrin-based coordination complexes: Syntheses, combined experimental and theoretical structures elucidation, spectroscopy, photophysical properties and antibacterial activity, Journal of Solid State Chemistry. 258 (2018) 477–484. https://doi.org/10.1016/j.jssc.2017.11.018.

[69] F.R. Kooriyaden, S. Sujatha, C. Arunkumar, Synthesis, spectral, structural and antimicrobial studies of fluorinated porphyrins, Polyhedron. 97 (2015) 66–74. https://doi.org/10.1016/j.poly.2015.05.018.
[70] B. Licina, E. Selimovic, T. Soldatovic, Antibacterial Activity of Zinc(II) and Copper(II) Terpyridine Complexes, in: Proceedings of 2nd International Electronic Conference on Medicinal Chemistry, MDPI, Sciforum.net, 2016: p. A002. https://doi.org/10.3390/ecmc-2-A002.
[71] B. Tweedy, Plant extracts with metal ions as potential antimicrobial agents, Phytopathology. 55 (1964) 910–914.
[72] S. Moghnie, A. Tovmasyan, J. Craik, I. Batinic-Haberle, L. Benov, Cationic amphiphilic Zn-porphyrin with high antifungal photodynamic potency, Photochem. Photobiol. Sci. 16 (2017) 1709–1716. https://doi.org/10.1039/C7PP00143F.
[73] G.D. Bajju, S. Kundan, M. Bhagat, D. Gupta, A. Kapahi, G. Devi, Synthesis and Spectroscopic and Biological Activities of Zn(II) Porphyrin with Oxygen Donors, Bioinorganic Chemistry and Applications. 2014 (2014) 1–13. https://doi.org/10.1155/2014/782762.
[74] U. Singh, A.M. Malla, I.A. Bhat, A. Ahmad, M.N. Bukhari, S. Bhat, S. Anayutullah, A.A. Hashmi, Synthesis, molecular docking and evaluation of antifungal activity of Ni(II),Co(II) and Cu(II) complexes of porphyrin core macromolecular ligand, Microbial Pathogenesis. 93 (2016) 172–179. https://doi.org/10.1016/j.micpath.2016.02.011.
[75] G. Karimipour, S. Kowkabi, A. Naghiha, New aminoporphyrins bearing urea derivative substituents: synthesis, characterization, antibacterial and antifungal activity, Braz. Arch. Biol. Technol. 58 (2015) 431–442. https://doi.org/10.1590/S1516-8913201500024.
[76] N. Dharmaraj, P. Viswanathamurthi, K. Natarajan, Ruthenium(II) complexes containing bidentate Schiff bases and their antifungal activity, Transition Metal Chemistry. 26 (2001) 105–109. https://doi.org/10.1023/A:1007132408648.
[77] C. Zhuang, X. Tang, D. Wang, A. Xia, W. Lian, Y. Shi, T. Shi, An unsymmetrical porphyrin and its metal complexes: Synthesis, spectroscopy, thermal analysis and liquid crystal properties, J Serb Chem Soc. 74 (2009) 1097–1104. https://doi.org/10.2298/JSC0910097Z.
[78] L. Mishra, V.K. Singh, Synthesis, structural and antifungal studies of Co (II), Ni (II), Cu (II) and Zn (II) complexes with new Schiff bases bearing benzimidazoles, (1993).
[79] C. Kontogiorgis, D. Hadjipavlou-Litina, Biological Evaluation of Several Coumarin Derivatives Designed as Possible Anti-inflammatory/Antioxidant Agents, Journal of Enzyme Inhibition and Medicinal Chemistry. 18 (2003) 63–69. https://doi.org/10.1080/1475636031000069291.
[80] R. Cini, G. Giorgi, A. Cinquantini, C. Rossi, M. Sabat, Metal complexes of the antiinflammatory drug piroxicam, Inorg. Chem. 29 (1990) 5197–5200. https://doi.org/10.1021/ic00351a012.
[81] R. Thangam, V. Suresh, S. Kannan, Optimized extraction of polysaccharides from Cymbopogon citratus and its biological activities, International Journal of Biological Macromolecules. 65 (2014) 415–423. https://doi.org/10.1016/j.ijbiomac.2014.01.033.
[82] Y. Carmona-Jiménez, M.V. García-Moreno, J.M. Igartuburu, C. Garcia Barroso, Simplification of the DPPH assay for estimating the antioxidant activity of wine and wine by-products, Food Chemistry. 165 (2014) 198–204. https://doi.org/10.1016/j.foodchem.2014.05.106.
[83] N. Amiri, S. Nouir, M. Hajji, T. Roisnel, T. Guerfel, G. Simonneaux, H. Nasri, Synthesis, structure, photophysical properties and biological activity of a cobalt(II) coordination complex with 4,4'-bipyridine and porphyrin chelating ligands, Journal of Saudi Chemical Society. 23 (2019) 781–794. https://doi.org/10.1016/j.jscs.2019.03.003.
[84] C. Hu, D.D. Kitts, Evaluation of antioxidant activity of epigallocatechin gallate in biphasic model systems in vitro, Molecular and Cellular Biochemistry. 218 (2001) 147–155. https://doi.org/10.1023/A:1007220928446.
[85] H. HAJ-HAMDO, W. KHAYATA, Z. AL-ASSAF, Estimating the antioxidant activity for natural antioxidants (tocochromanol) and synthetic one by DPPH, International Journal of Pharmacy and Pharmaceutical Sciences. 5 (2014) 441–444.
[86] M. Hajji, N. Amiri, F. Ben Taheur, A. Bujacz, H. Nasri, T. Guerfel, Heteroleptic cobalt(II) complex with nitrogen-rich macrocycles — Structure, bioactivity and DFT modelling, Solid State Sciences. 100 (2020) 106117. https://doi.org/10.1016/j.solidstatesciences.2020.106117.

[87] N. Amiri, F. Ben Taheur, S. Chevreux, C.M. Rodrigues, V. Dorcet, G. Lemercier, H. Nasri, Syntheses, crystal structures, photo-physical properties, antioxidant and antifungal activities of Mg(II) 4,4'-bipyridine and Mg(II) pyrazine complexes of the 5,10,15,20 tetrakis(4–bromophenyl)porphyrin, Inorganica Chimica Acta. 525 (2021) 120466. https://doi.org/10.1016/j.ica.2021.120466.
[88] M. Aydın, E.H. Alıcı, A.T. Bilgiçli, M.N. Yarasir, G. Arabaci, Synthesis, characterization, aggregation, fluorescence and antioxidant properties of bearing (4-(methylthio)phenylthio) tetra substituted phthalocyanines, Inorganica Chimica Acta. 464 (2017) 1–10. https://doi.org/10.1016/j.ica.2017.04.038.
[89] N. Söylemez, E. Yabaş, S.Ş. Bölükbaşı, M. Sülü, Antioxidant activities of the new tetrasubstituted metal-free, Zn(II) and Co(II) monophthalocyanines, J. Porphyrins Phthalocyanines. 22 (2018) 233–242. https://doi.org/10.1142/S1088424618500190.
[90] N. Yıldırım, A.T. Bilgiçli, E.H. Alici, G. Arabacı, M.N. Yarasir, Formation, characterization, aggregation, fluorescence and antioxidant properties of novel tetrasubstituted metal-free and metallophthalocyanines bearing (4-(methylthio)phenoxy) moieties, Journal of Molecular Structure. 1144 (2017) 66–79. https://doi.org/10.1016/j.molstruc.2017.05.006.
[91] M. Baranowska, K. Suliborska, W. Chrzanowski, B. Kusznierewicz, J. Namieśnik, A. Bartoszek, The relationship between standard reduction potentials of catechins and biological activities involved in redox control, Redox Biology. 17 (2018) 355–366. https://doi.org/10.1016/j.redox.2018.05.005.
[92] L. Díaz-Rubio, R. Hernández-Martínez, A. Estolano-Cobián, D. Chávez-Velasco, R. Salazar-Aranda, N. Waksman de Torres, I. Rivero, V. García-González, M. Ramos, I. Córdova-Guerrero, Synthesis, Biological Evaluation and Docking Studies of Chalcone and Flavone Analogs as Antioxidants and Acetylcholinesterase Inhibitors, Applied Sciences. 9 (2019) 410. https://doi.org/10.3390/app9030410.
[93] I. Nakanishi, T. Kawashima, K. Ohkubo, H. Kanazawa, K. Inami, M. Mochizuki, K. Fukuhara, H. Okuda, T. Ozawa, S. Itoh, S. Fukuzumi, N. Ikota, Electron-transfer mechanism in radical-scavenging reactions by a vitamin E model in a protic medium, Org. Biomol. Chem. 3 (2005) 626. https://doi.org/10.1039/b416572a.
[94] O. Friaa, D. Brault, Kinetics of the reaction between the antioxidant Trolox® and the free radical DPPH$^{\cdot}$ in semi-aqueous solution, Org. Biomol. Chem. 4 (2006) 2417. https://doi.org/10.1039/b602147f.
[95] L. Tabrizi, T.L.A. Nguyen, D.Q. Dao, Experimental and theoretical investigation of cyclometalated phenylpyridine iridium(III) complex based on flavonol and ibuprofen ligands as potent antioxidant, RSC Adv. 9 (2019) 17220–17237. https://doi.org/10.1039/C9RA02726B.